Supplementary Information for "The effectiveness of solar radiation management for marine cloud brightening geoengineering by fine sea spray in worldwide different climatic regions"

Zhe Song[1*], Shaocai Yu[2,3*+], Pengfei Li[4+], Ningning Yao[3,2], Lang Chen[3,2], Yuhai Sun[2], Boqiong Jiang[2], Daniel Rosenfeld[5]

[1] Research Center for Air Pollution and Health; Key Laboratory of Environmental Remediation and Ecological Health, Ministry of Education, College of Environment and Resource Sciences, Zhejiang University, Hangzhou, Zhejiang 310058, P.R. China

[2] Zhejiang Province Key Laboratory of Solid Waste Treatment and Recycling; School of Environmental Sciences and Engineering, Zhejiang Gongshang University, Hangzhou 310018, China

[3] School of Statistics and Mathematics, Zhejiang Gongshang University, Hangzhou 310018, China

[4] State Key Laboratory of Infrared Physics, Shanghai Institute of Technical Physics, Chinese Academy of Sciences, Shanghai 200031, China

[5] Institute of Earth Sciences, The Hebrew University of Jerusalem, Jerusalem, Israel

[*]Equal contribution

[+]*Correspondence to*: Shaocai Yu (shaocaiyu@zjgsu.edu.cn)，Pengfei Li (pengfeili@mail.sitp.ac.cn)

This file includes:

Text S1 to S2
Figures S1 to S28
Tables S1 to S3

Supplementary Text S1

We use the method of Martin et al. (1994) to calculate the cloud effective radius:

$$r_e = \left(\frac{3q_L}{4\pi\rho_w k N_{tot}}\right)^{\frac{1}{3}}$$

where q_L is the liquid water content, ρ_w is the density of water, N_{tot} is the cloud droplet number concentration (CDNC), and k is the ratio between the cube of the mean volume radius and the cube of the effective radius. Martin et al. (1994) estimated k for unpolluted (marine) stratocumulus clouds to be equal to 0.80 and for polluted (continental) stratocumulus clouds to be equal to 0.67. Here, we refer to the method of Goddard et al. (2022) and similarly set k to 0.80 for cloud condensation nuclei (CCN) concentrations of 0–50 cm^{-3} at 0.1% saturation, 0.74 for CCN concentrations of 50–150 cm^{-3} and equal to 0.67 where CCN concentrations are greater than 150 cm^{-3}.

We use the method of Wood (2007) and Stephens (1978) to approximate the column cloud optical thickness (COT):

$$\tau \approx \frac{3}{2}\int_{z=0}^{h} \frac{q_L(z)}{\rho_w r_e(z)} dz$$

when integrated from the surface to a specified height, h. The height is determined by the highest grid cell containing a liquid cloud (Goddard et al., 2022).

We use the method of Schwartz et al. (2002) to approximate the column mean cloud albedo:

$$\alpha_c \approx \frac{\tau(1-g) + 0.097}{\tau(1-g) + 1.43}$$

where g is the asymmetry parameter we assume g to be 0.834 for $r_e \leq 6$ μm, 0.873 for $r_e \geq 19$ μm, and to increase linearly between these re boundaries (Goddard et al., 2022).

Supplementary Text S2

The direct radiative effect of aerosols is mainly determined by their own optical properties. In WRF-CMAQ, the emitted sea-salt aerosol particle size distributions are adjusted to the local relative humidity (Kelly et al., 2010; Zhang et al., 2005). The dry diameter of sea-salt aerosols injected into the five regions is about 0.11–0.15 μm (Figs. 1a and S9), and the wet diameter is about 0.22–0.3 μm (Fig. S10). The single scattering albedo (SSA) of aerosols describes the ratio of aerosol particles' ability to absorb and scatter solar radiations. After the injection of sea-salt aerosols, the SSA of the accumulation mode aerosols in the five regions generally increases by about 0.003–0.005, and in some regions within the area, the SSA increases by over 0.007, with an average increase of 0.001–0.003 in sensitive areas (Fig. S11). This indicates that the injected sea-salt aerosol particles could scatter sunlight more effectively than absorb it, causing solar radiation to be reflected back into space. The asymmetry factor of aerosols is a parameter describing the directionality of aerosol particle scattering of sunlight, and an important factor for evaluating direct aerosol radiative forcing (Zhao et al., 2018). The injection of sea-salt aerosols in the five regions reduces the asymmetry factor by 0.007–0.029, with an average reduction of 0.01–0.027 in sensitive areas (Fig. S12). This indicates that the injected sea-salt aerosols tend to scatter more uniformly or backward rather than in a forward direction.

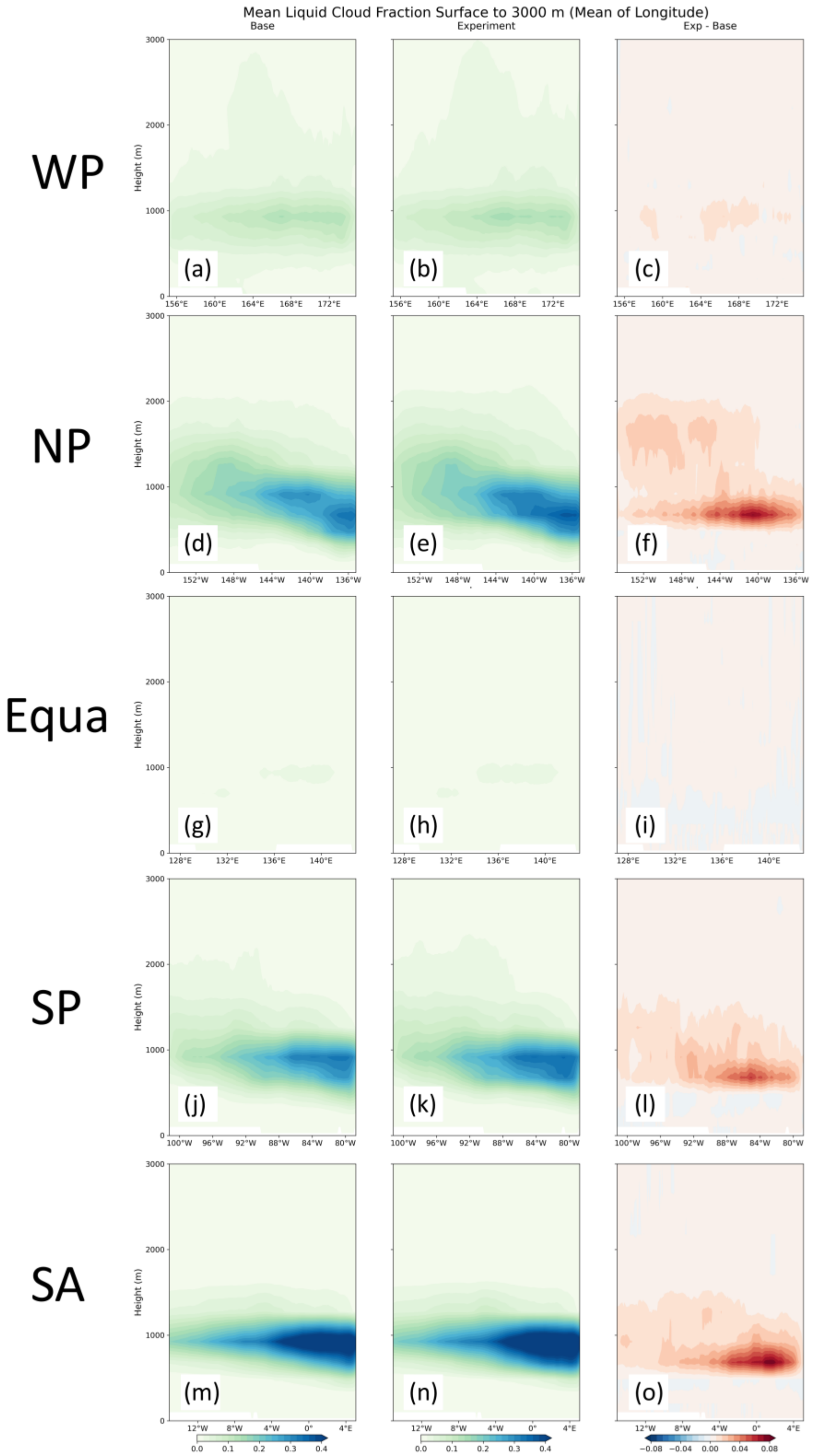

Figure S1. Vertical cross sections of the mean liquid cloud fraction from the surface to 3000 m altitude for five regions, with cross sections longitudinally averaged. The first to third columns are Base, the sensitivity experiment with a uniform injection of 10^{-9} kg m^{-2} s^{-1} of sea-salt aerosols over the entire region, and Exp - Base, respectively.

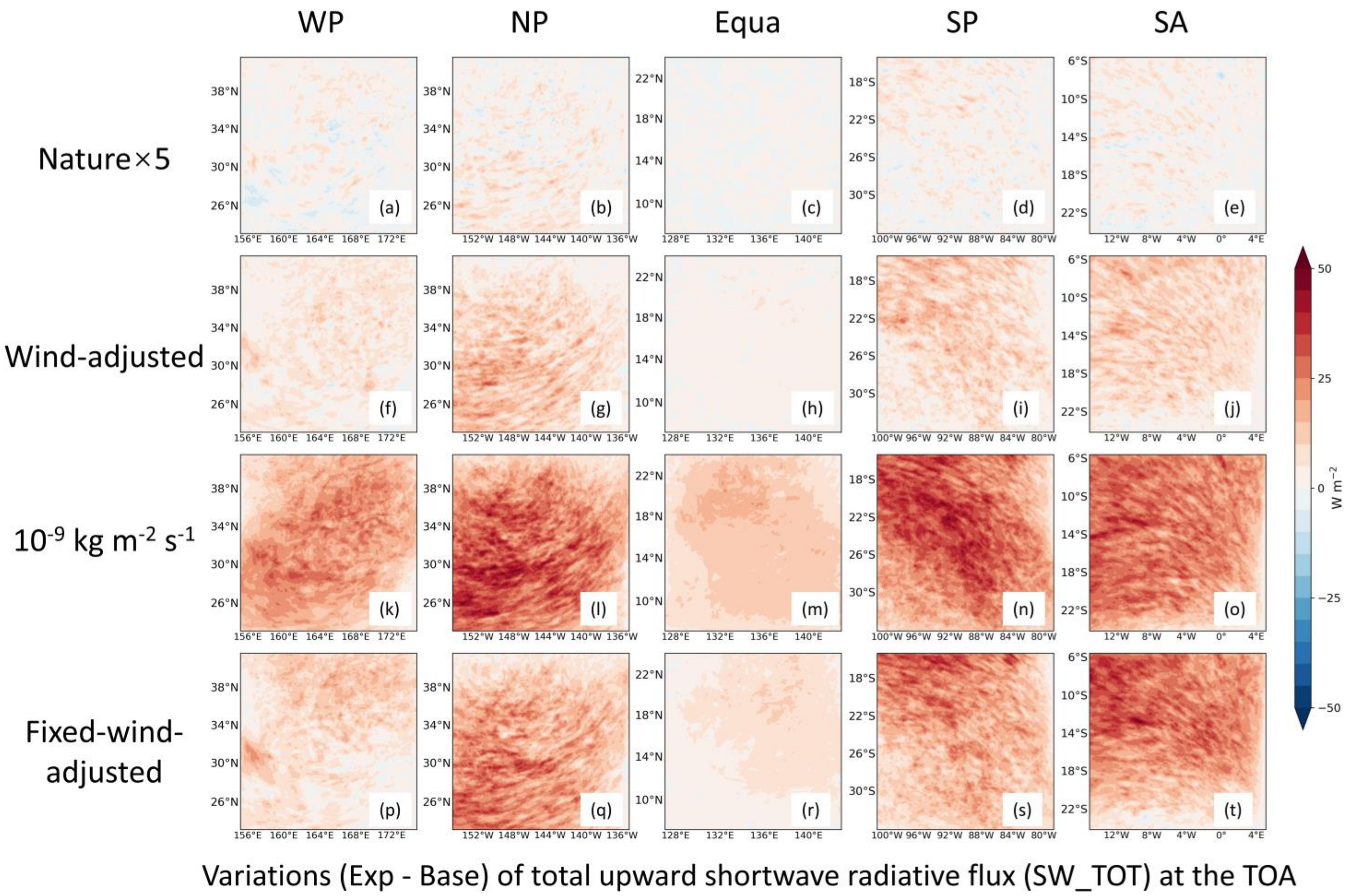

Figure S2. Spatial distribution of the differences (Exp - Base) in the SW_TOT at the TOA due to the injection of sea-salt aerosols in different ways in five oceanic regions.

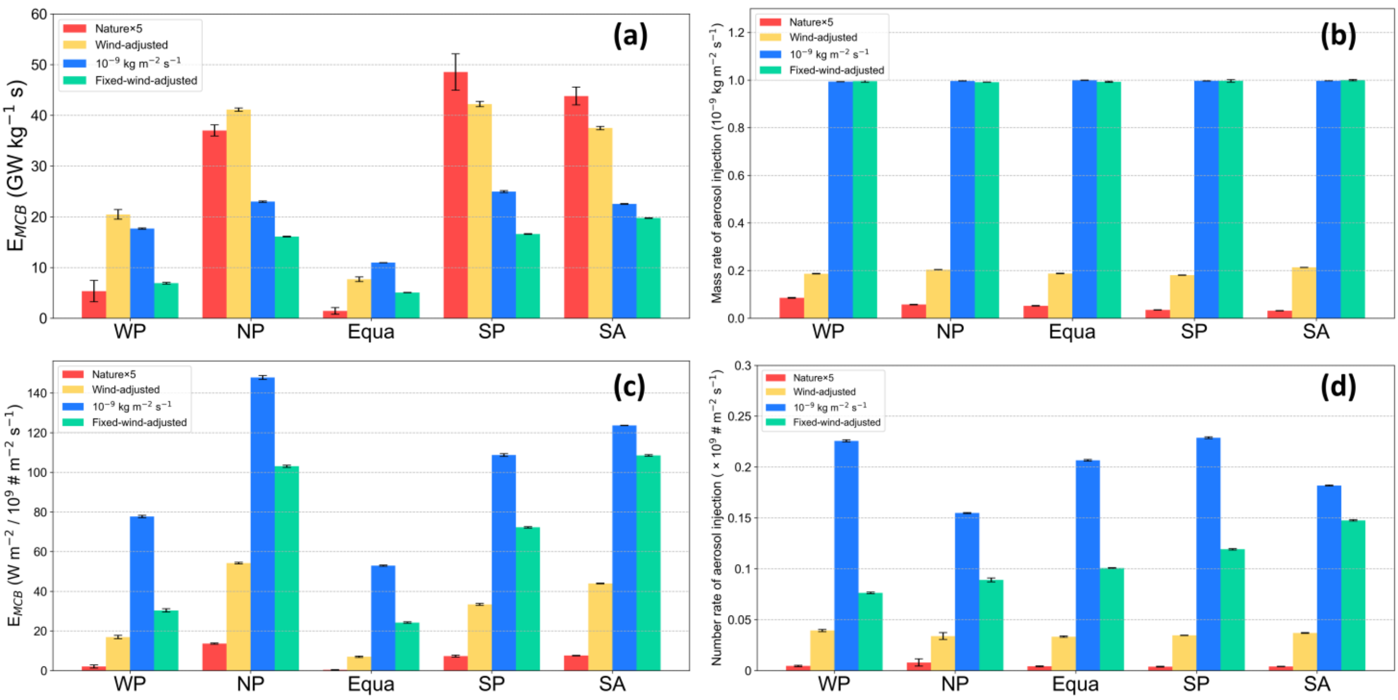

Figure S3. The MCB efficiency (**a**) and injection rates (**b**) in terms of aerosol mass, and MCB efficiency (**c**) and injection rates (**d**) in terms of aerosol number across different strategies in five ocean regions.

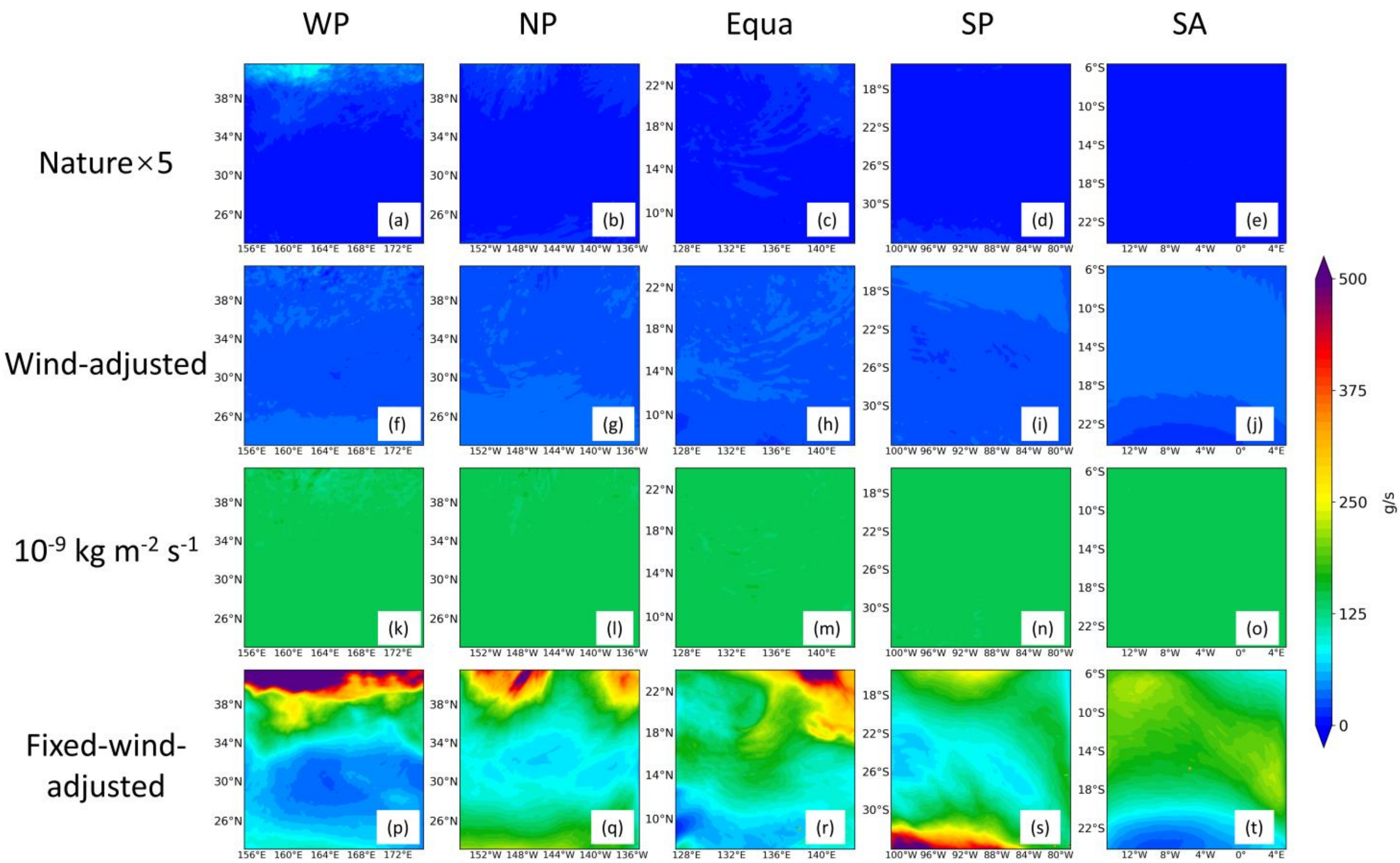

Figure S4. Spatial distribution of the differences (Exp - Base) in the sea-salt emissions due to the injection of sea-salt aerosols in different ways in five oceanic regions.

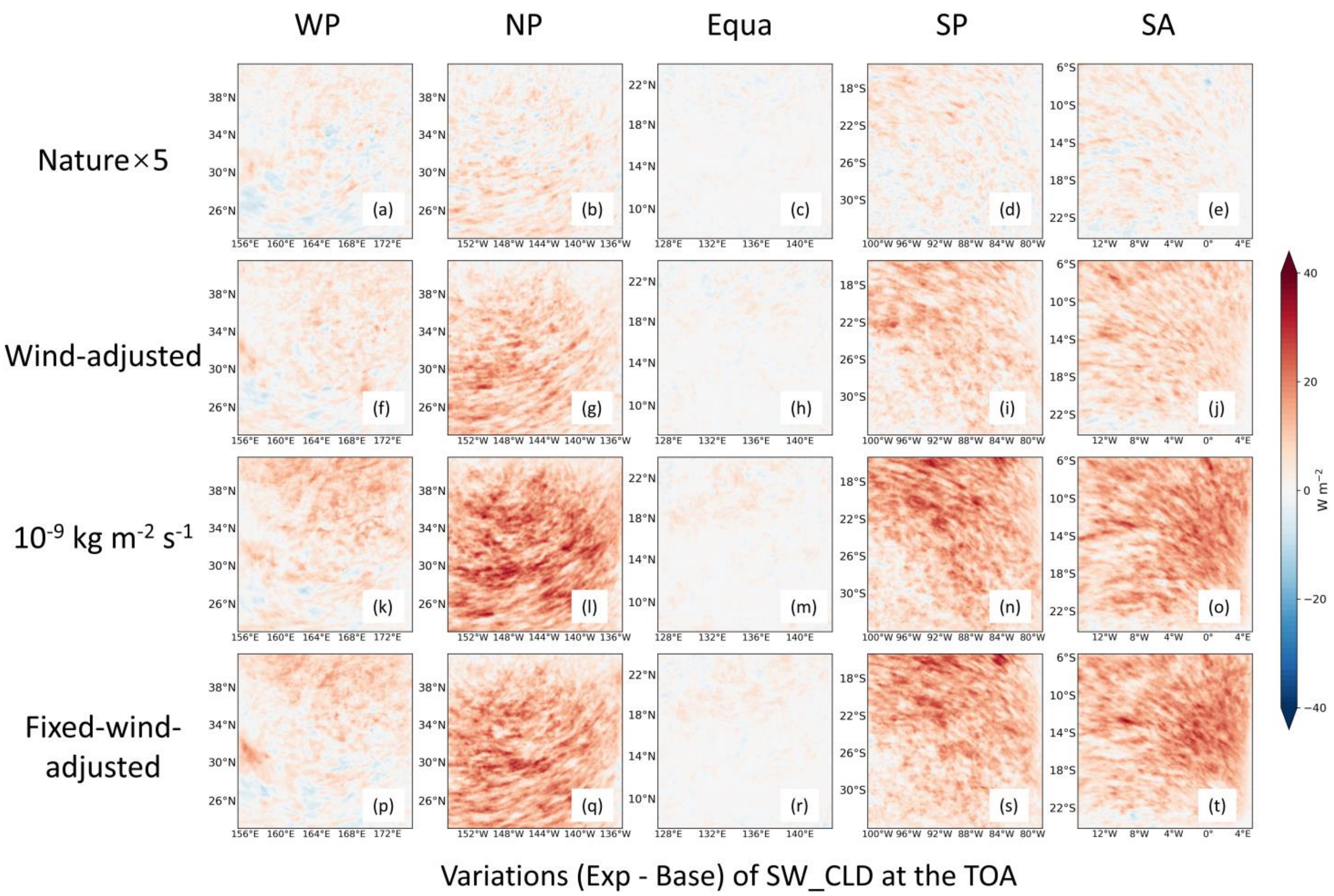

Figure S5. Same caption as Fig. S2, but for the results of SW_CLD (W m^{-2}).

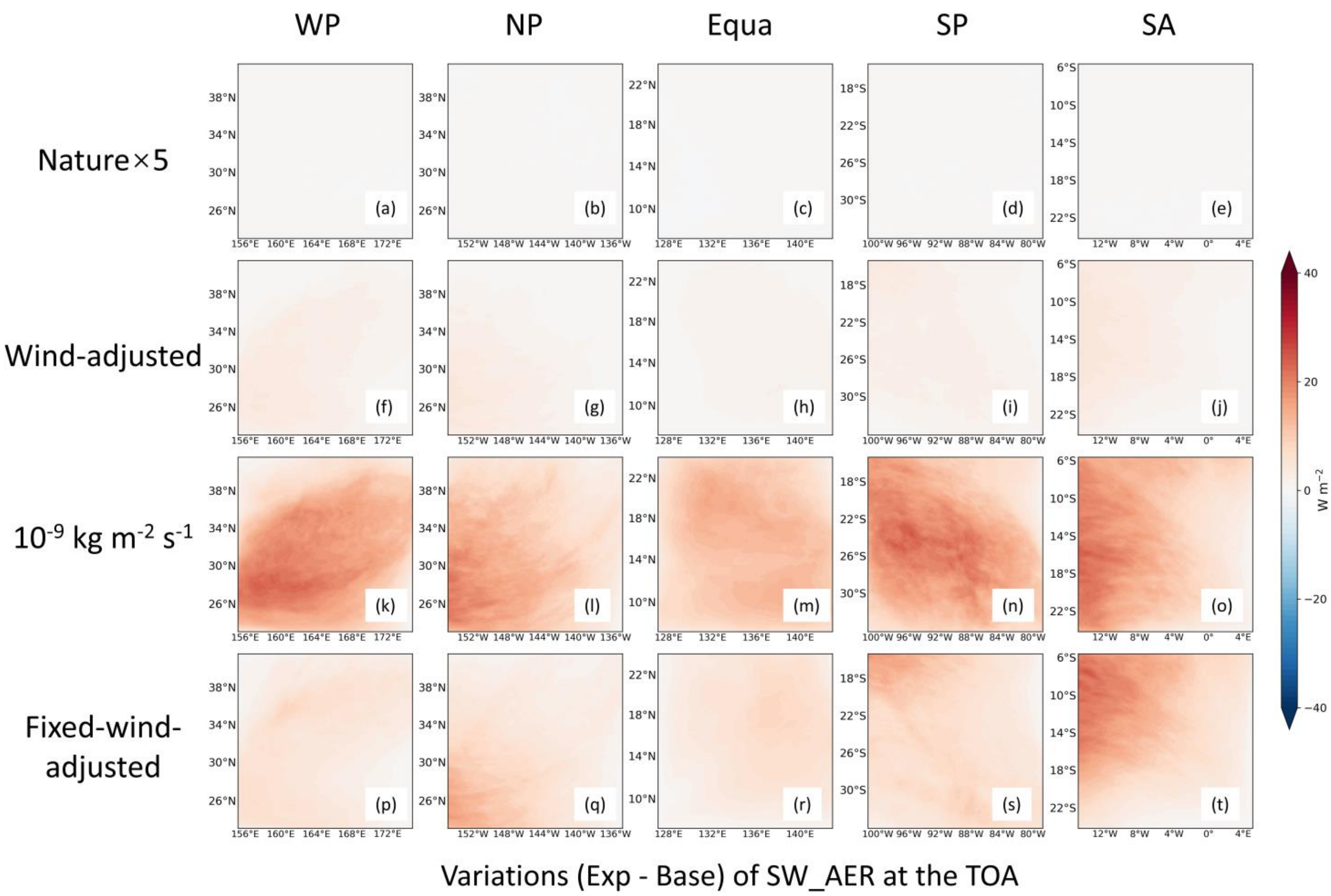

Figure S6. Same caption as Fig. S2, but for the results of SW_AER (W m^{-2}).

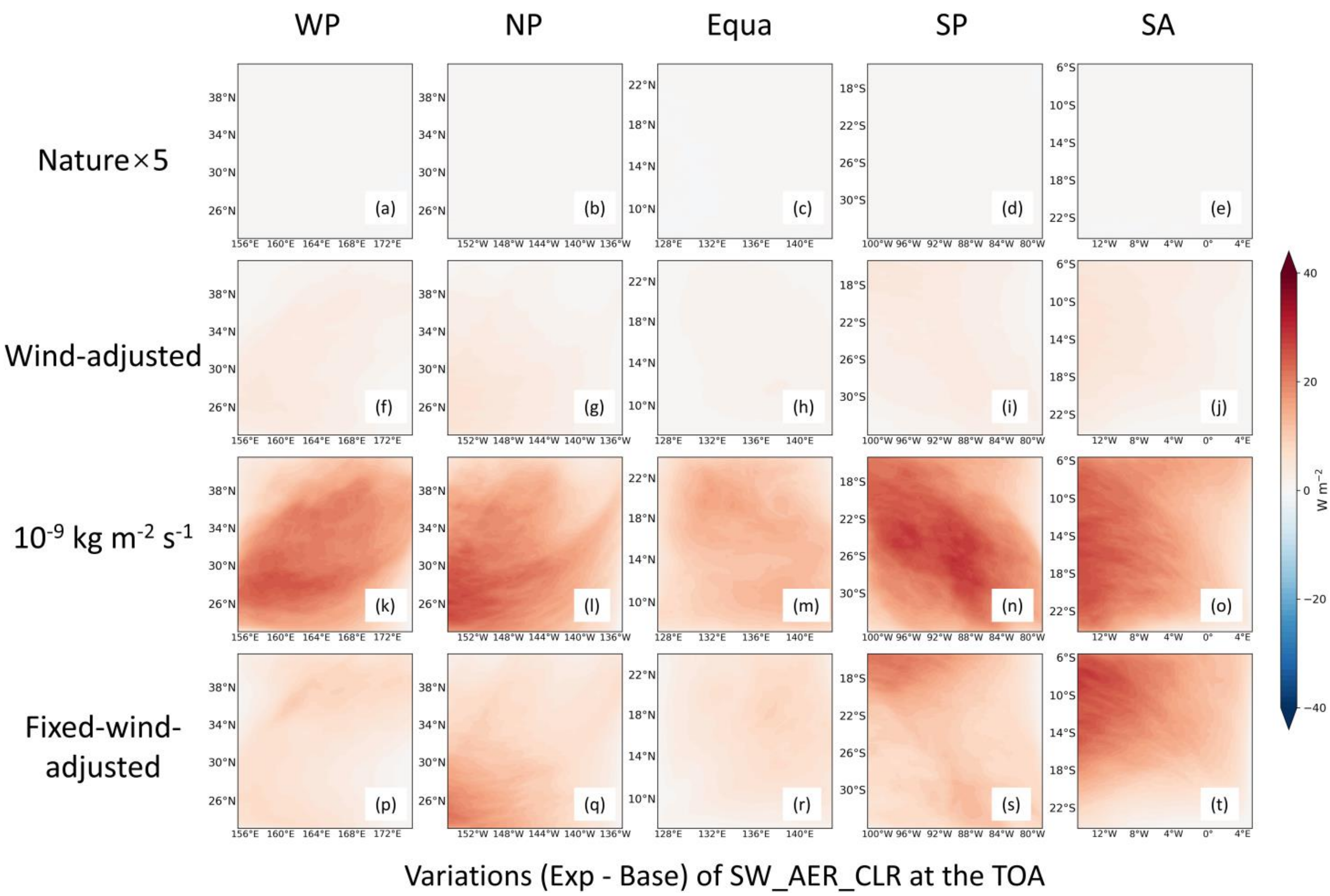

Figure S7. Same caption as Fig. S2, but for the results of SW_AER_CLR (W m^{-2}).

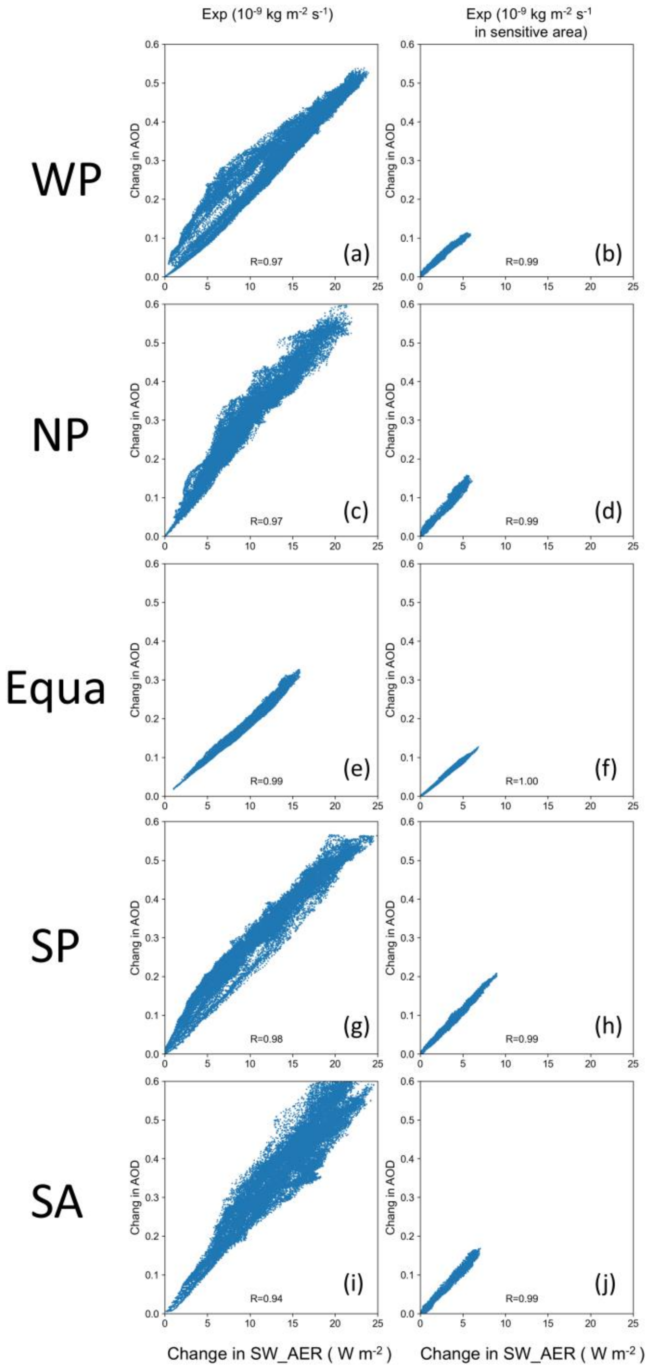

Figure S8. Relationship between changes in AOD and SW_AER responses due to uniform injection of 10^{-9} kg m^{-2} s^{-1} sea-salt aerosols over the entire region (first column) and injection only within sensitive areas (second column). The Pearson's correlation coefficient (R) is given for each relationship.

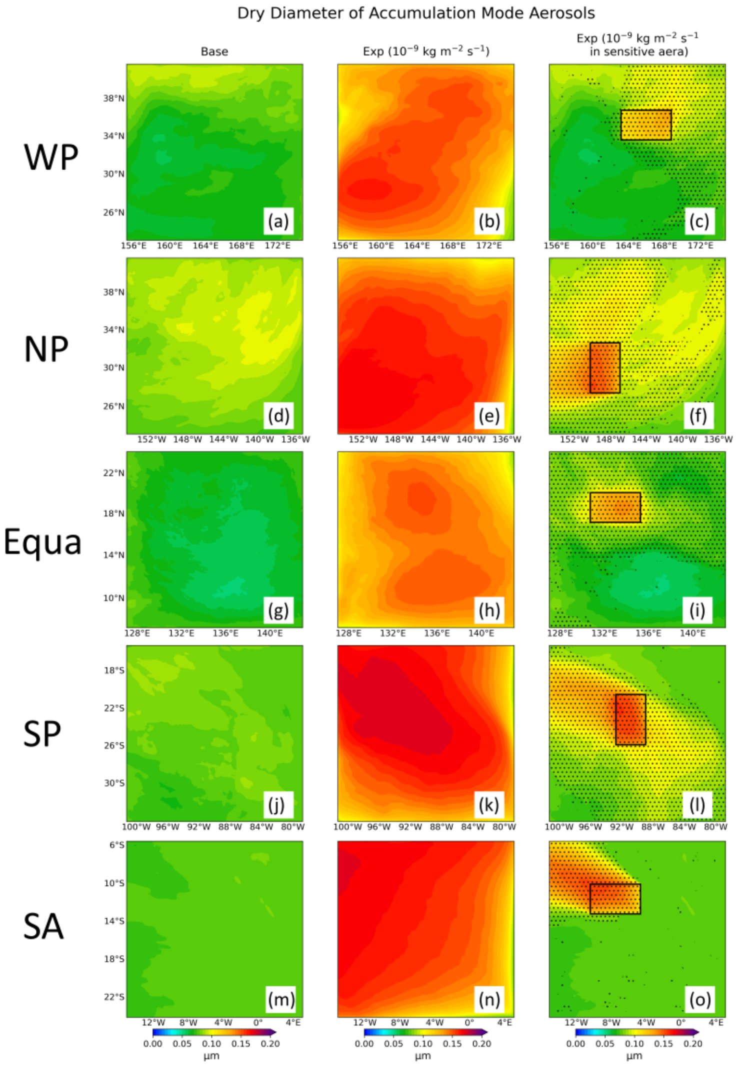

Figure S9. Spatial distribution of dry diameter of accumulation mode aerosols for five ocean regions. The first column is for Base, the second is for sensitivity experiments with uniform injections of 10^{-9} kg m^{-2} s^{-1}, and the third is for sensitivity experiments after uniform injections in sensitive areas. Areas labeled with dots indicate mean differences that are significant at the 95% confidence level. The black rectangles are sensitive areas.

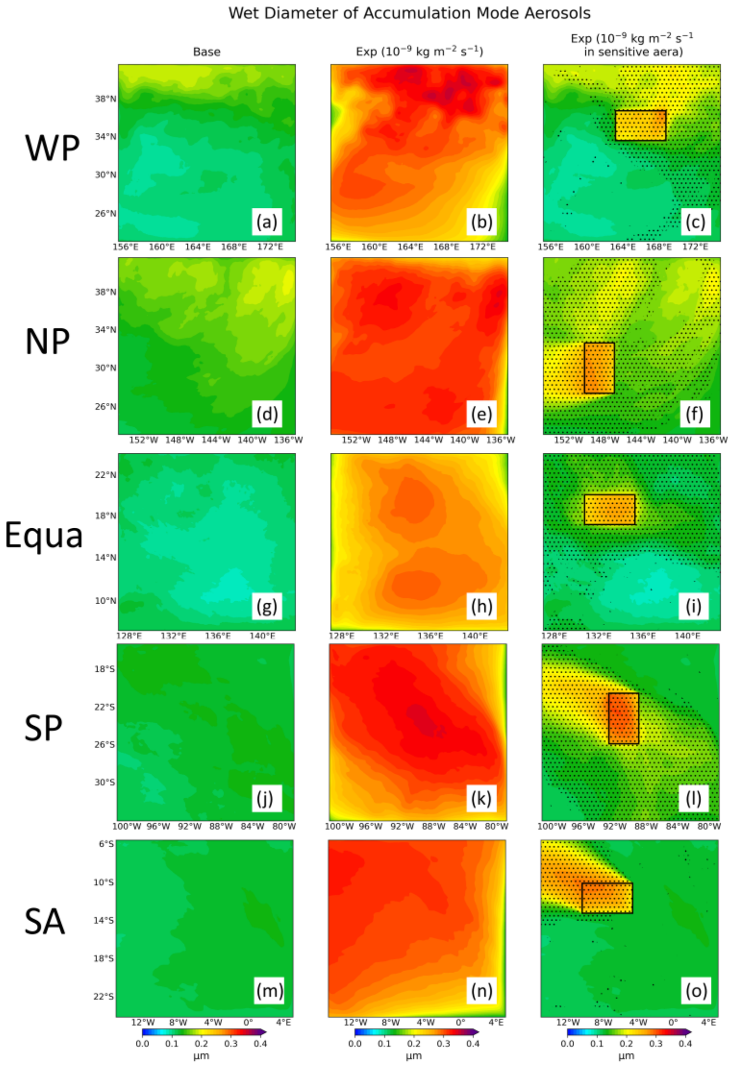

Figure S10. Same caption as Fig. S9, but for the wet diameter of accumulation mode aerosols.

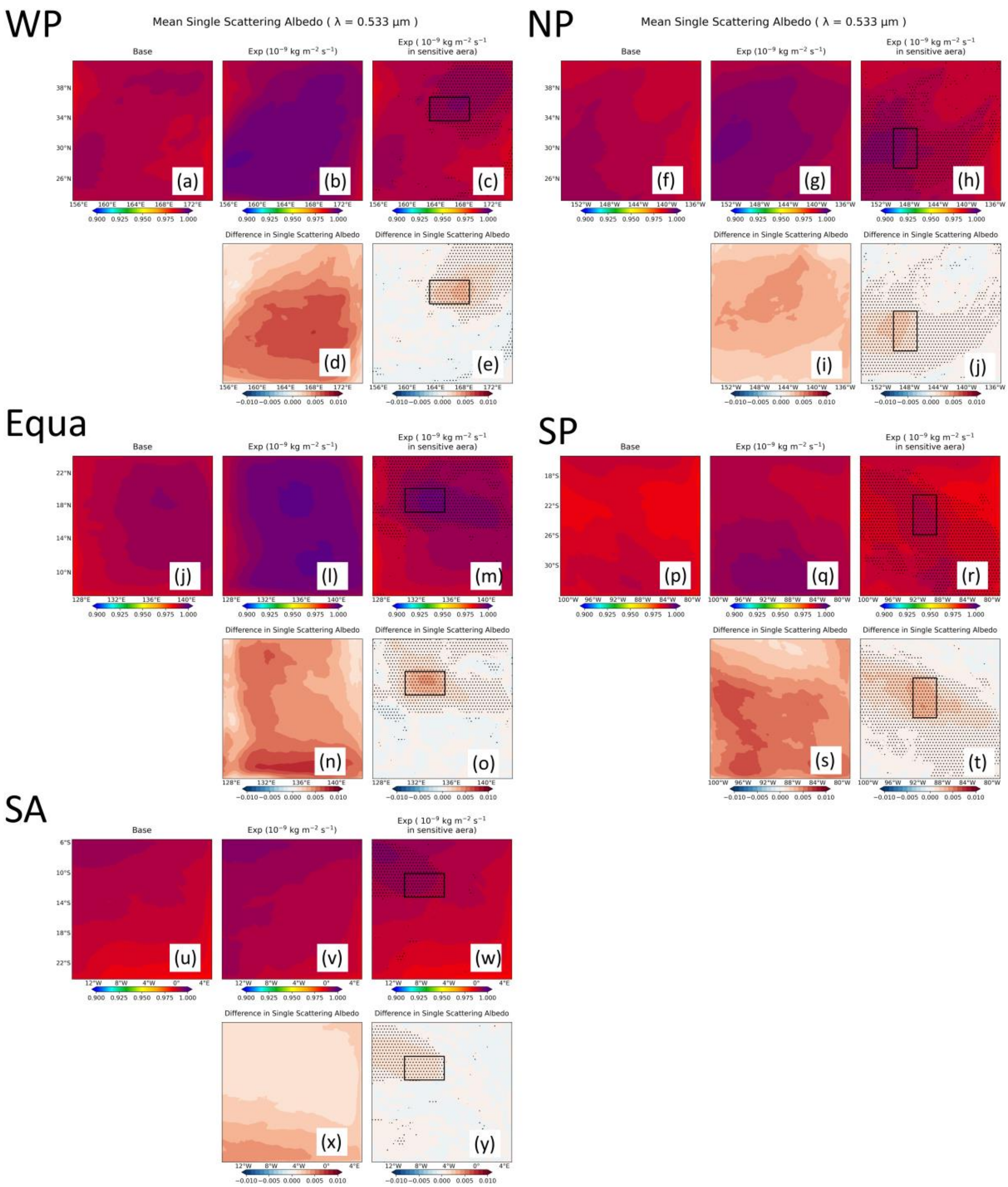

Figure S11. Spatial distribution of aerosol single scattering albedo (λ = 0.533μm) for Base and sensitivity experiments in five regions. The first row for each region shows the results for Base, the sensitivity experiment with a uniform injection of 10^{-9} kg m^{-2} s^{-1}, and the sensitivity experiment with a uniform injection in the sensitive area. The second row shows the difference between the sensitivity experiment and Base (Exp - Base), respectively. Areas labeled with dots indicate mean differences that are significant at the 95% confidence level. The black rectangles are sensitive areas.

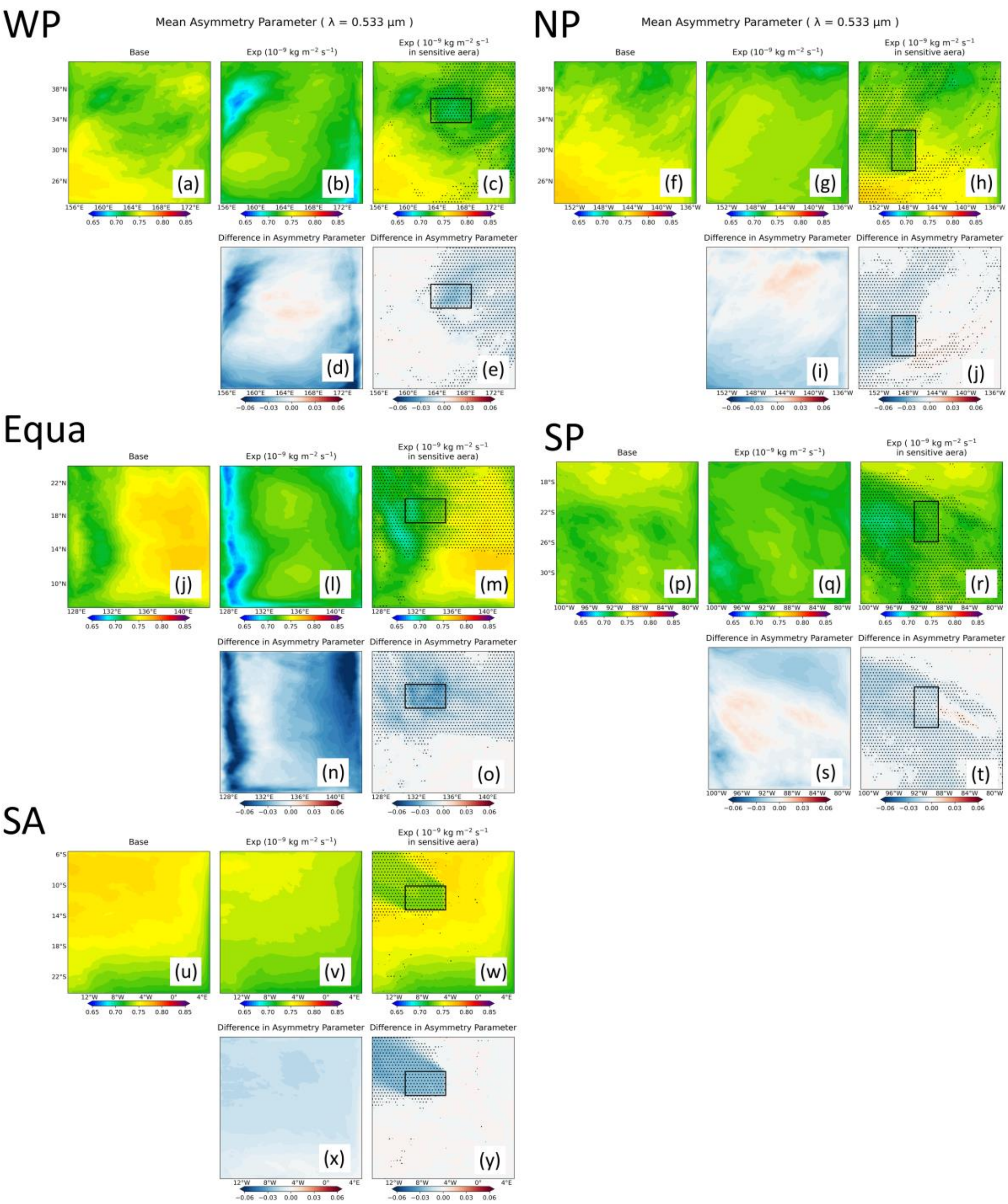

Figure S12. Same caption as Fig. S11, but for the aerosol asymmetry factor.

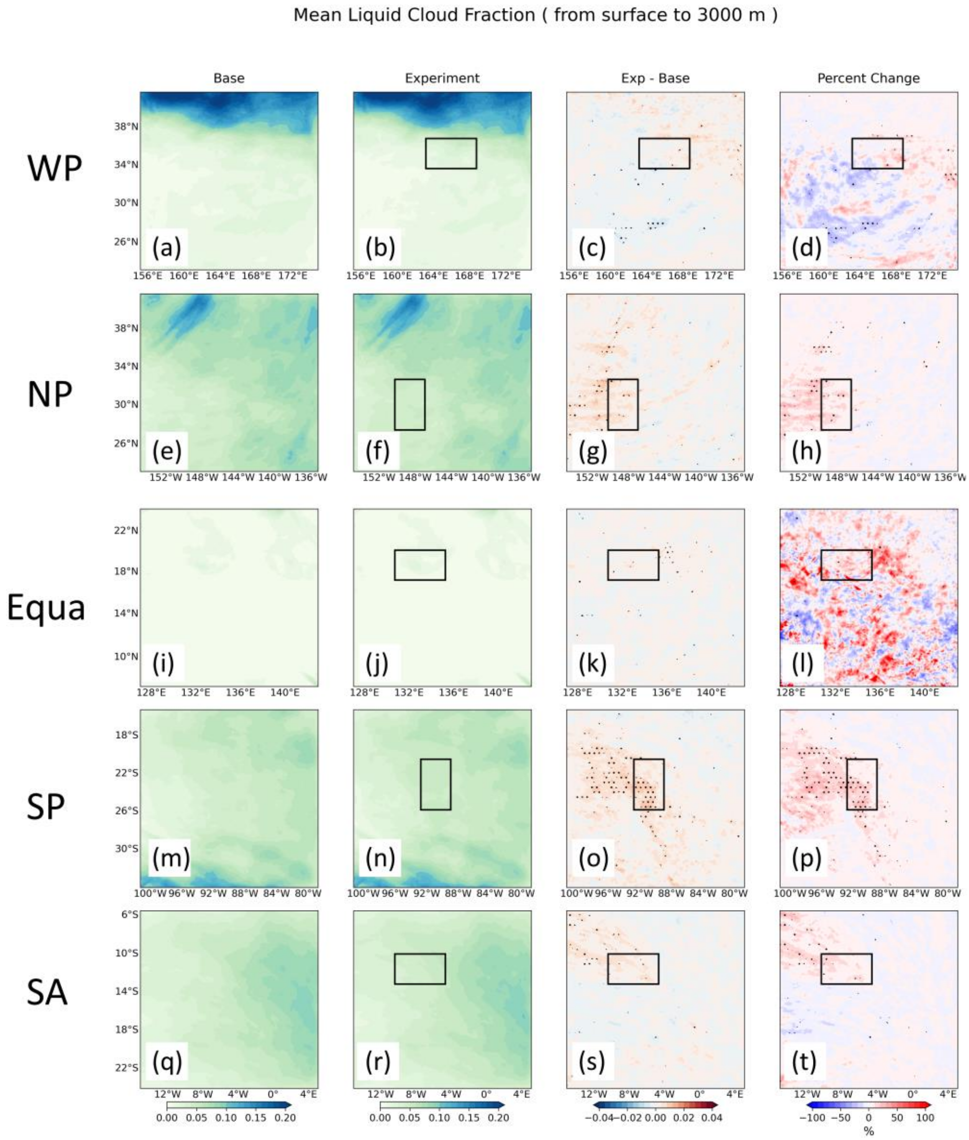

Figure S13. Same caption as Fig. 2, but for the sensitivity experiment with a uniform injection of 10^{-9} kg m^{-2} s^{-1} sea-salt aerosols only in the sensitive area. Areas labeled with dots indicate mean differences that are significant at the 95% confidence level. The black rectangles are sensitive areas.

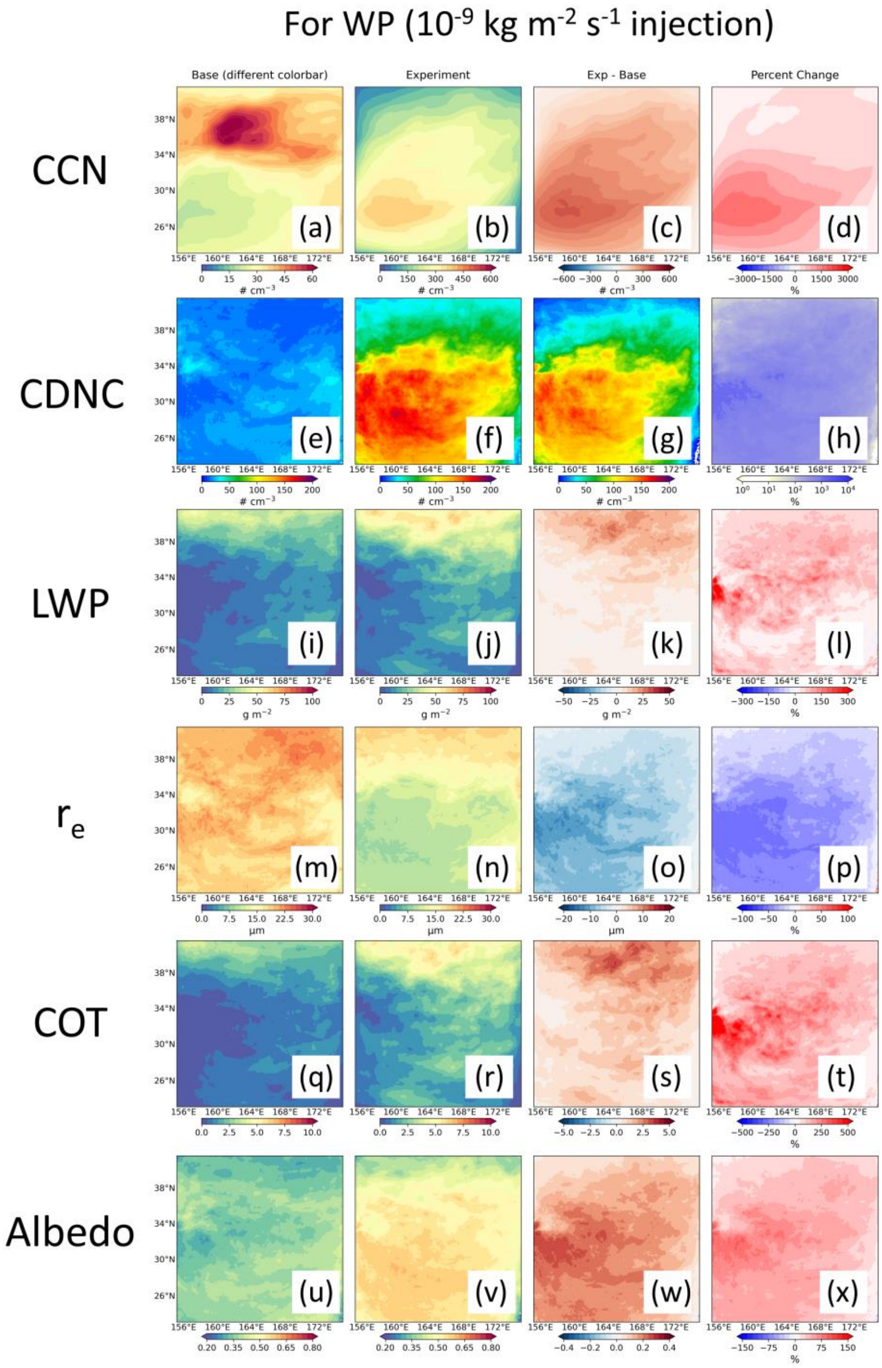

Figure S14. Same caption as Fig. 10, but for the WP region.

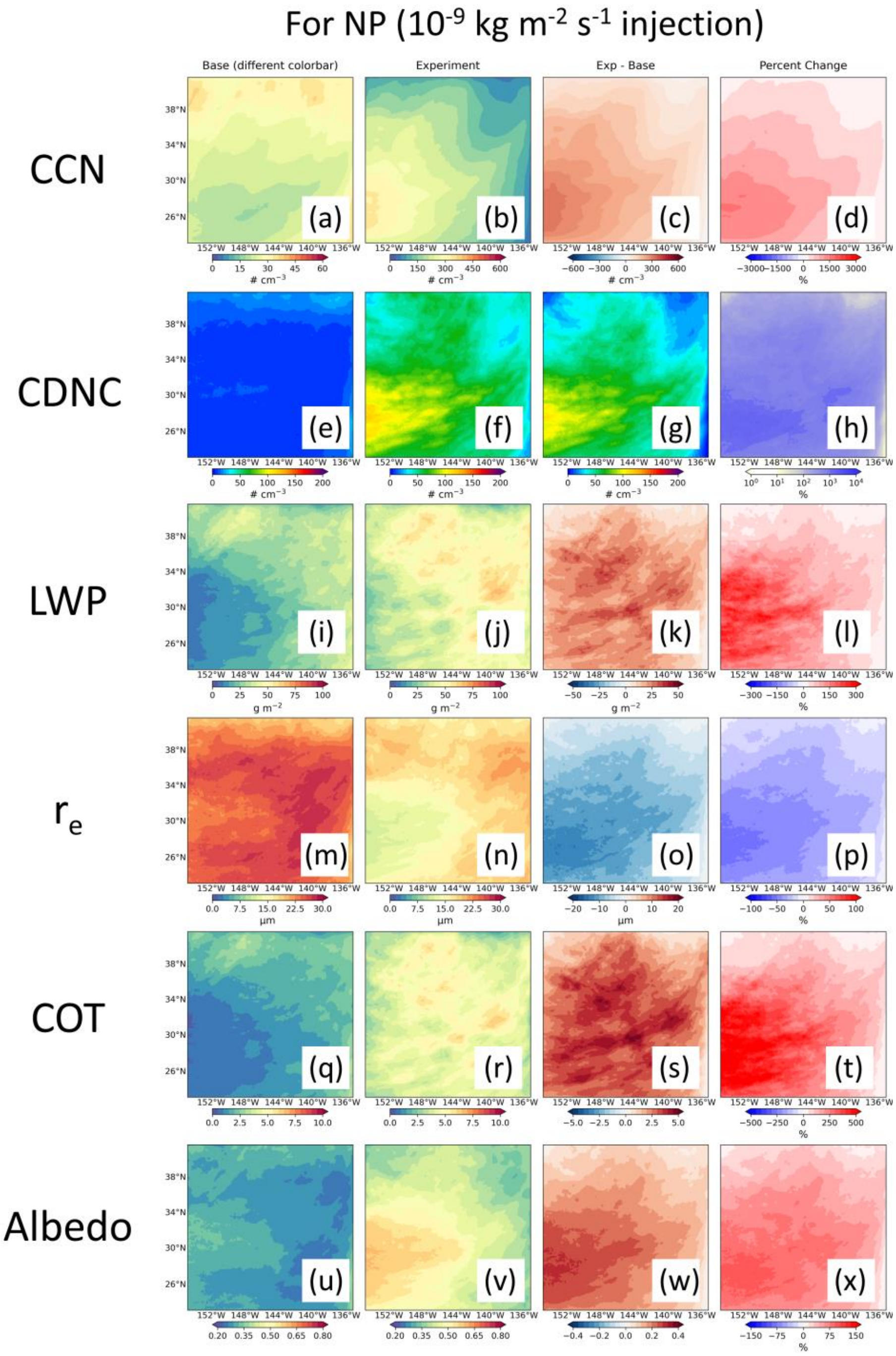

Figure S15. Same caption as Fig. 10, but for the NP region.

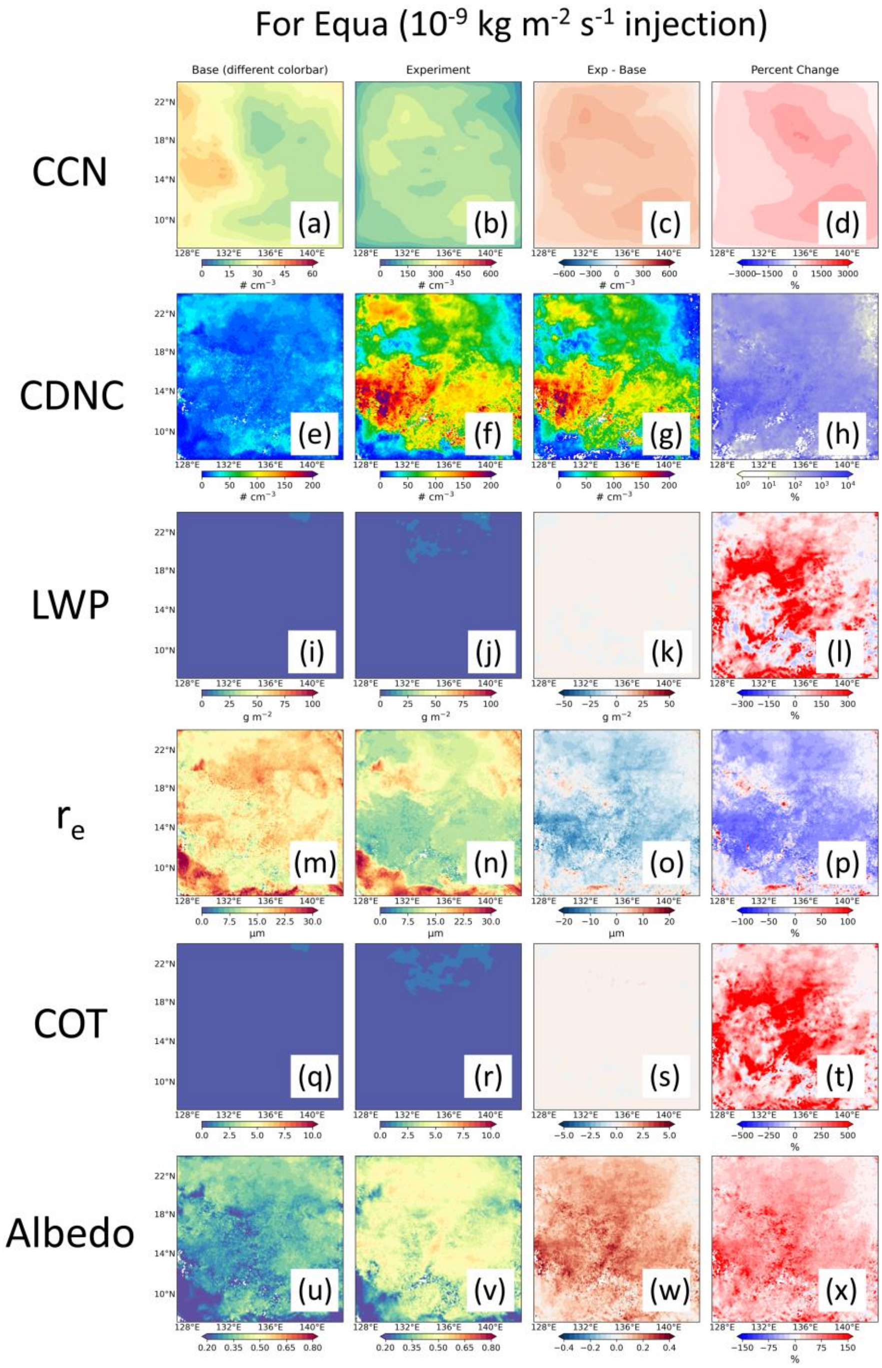

Figure S16. Same caption as Fig. 10, but for the Equa region.

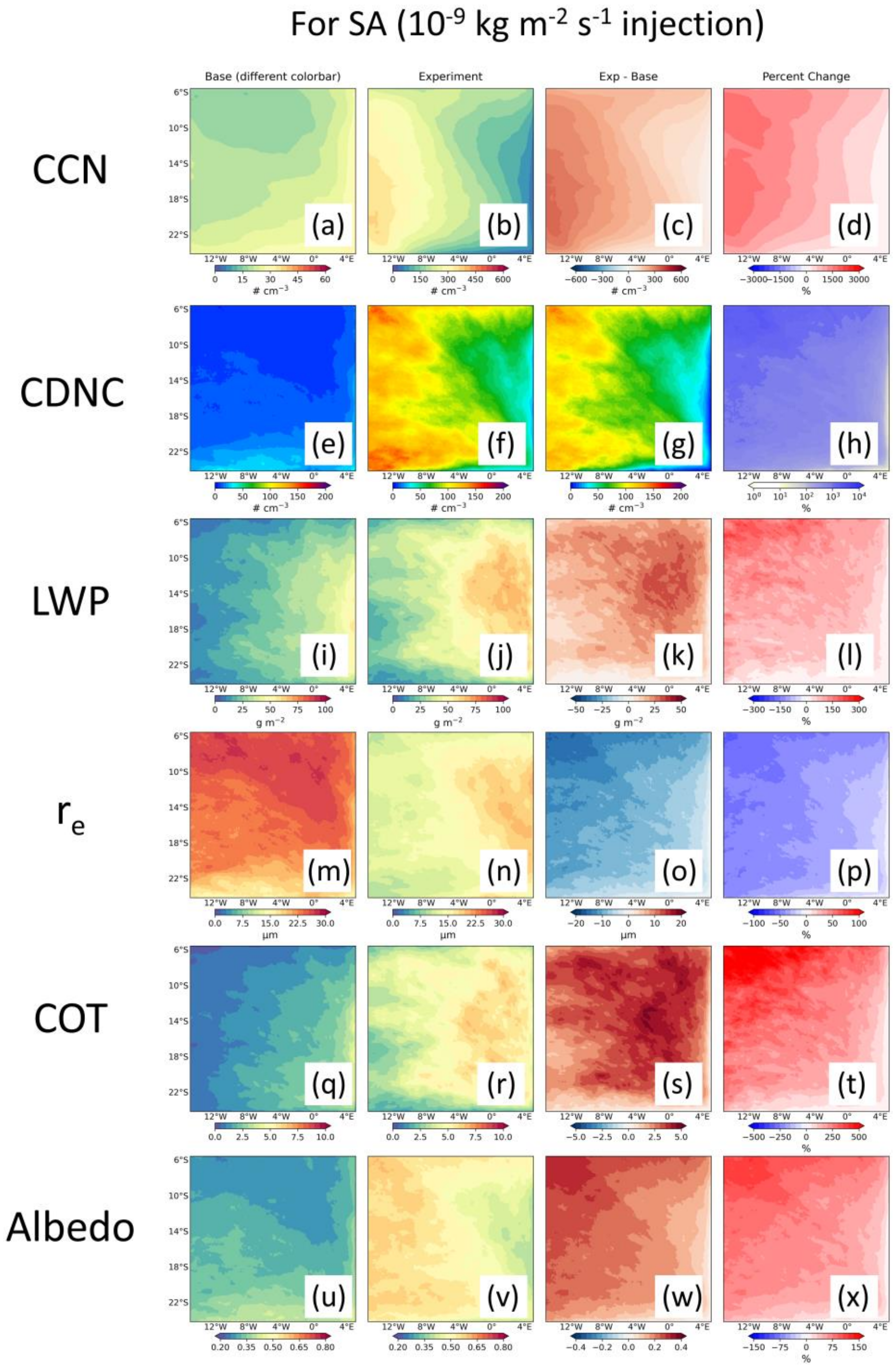

Figure S17. Same caption as Fig. 10, but for the SA region.

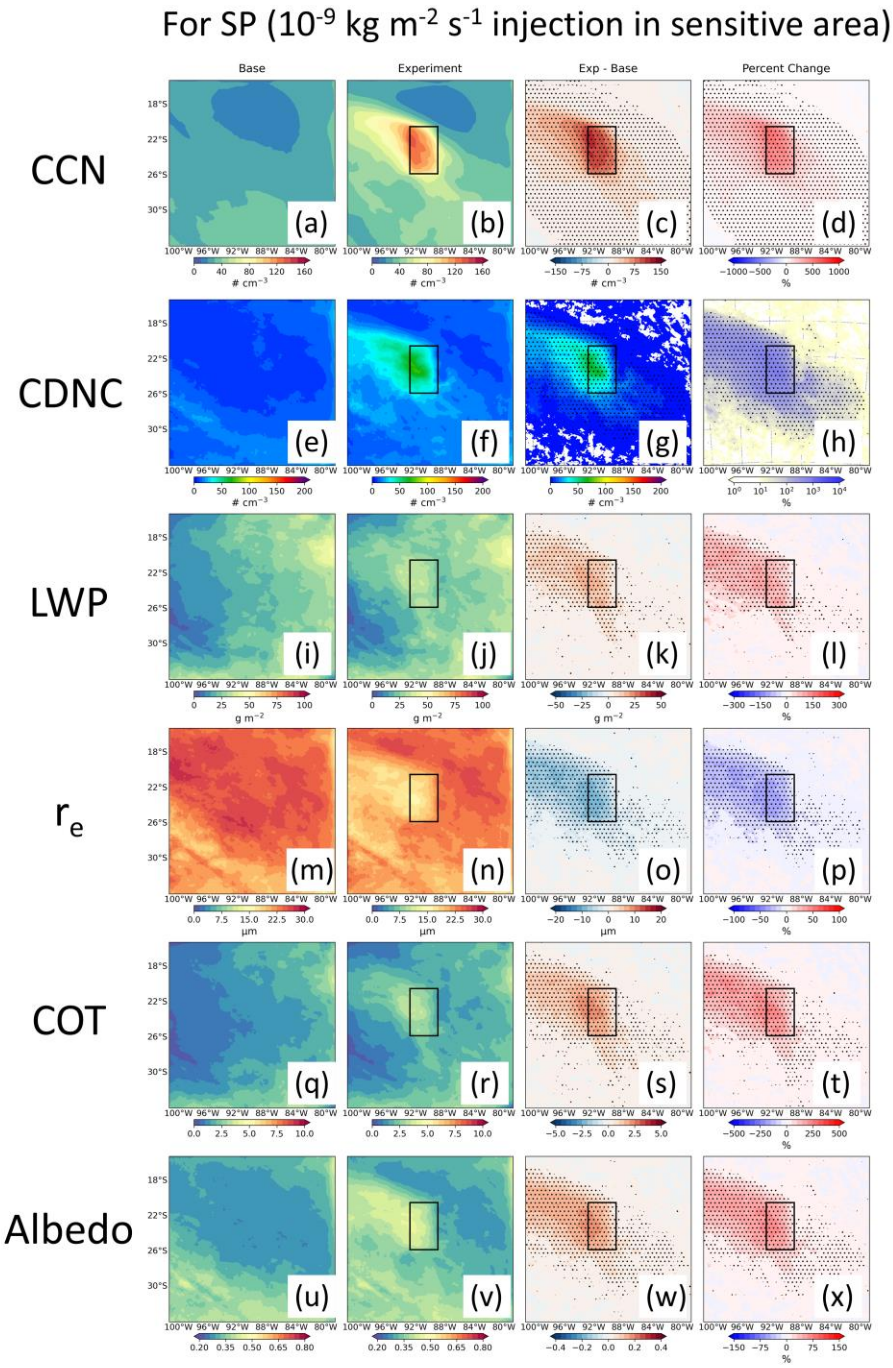

Figure S18. Same caption as Fig. 10, but showing the spatial distribution of the liquid cloud property response to a uniform injection of sea-salt aerosols within the sensitive area in the SP. Areas labeled with dots indicate mean differences that are significant at the 95% confidence level. The black rectangles are the sensitive areas.

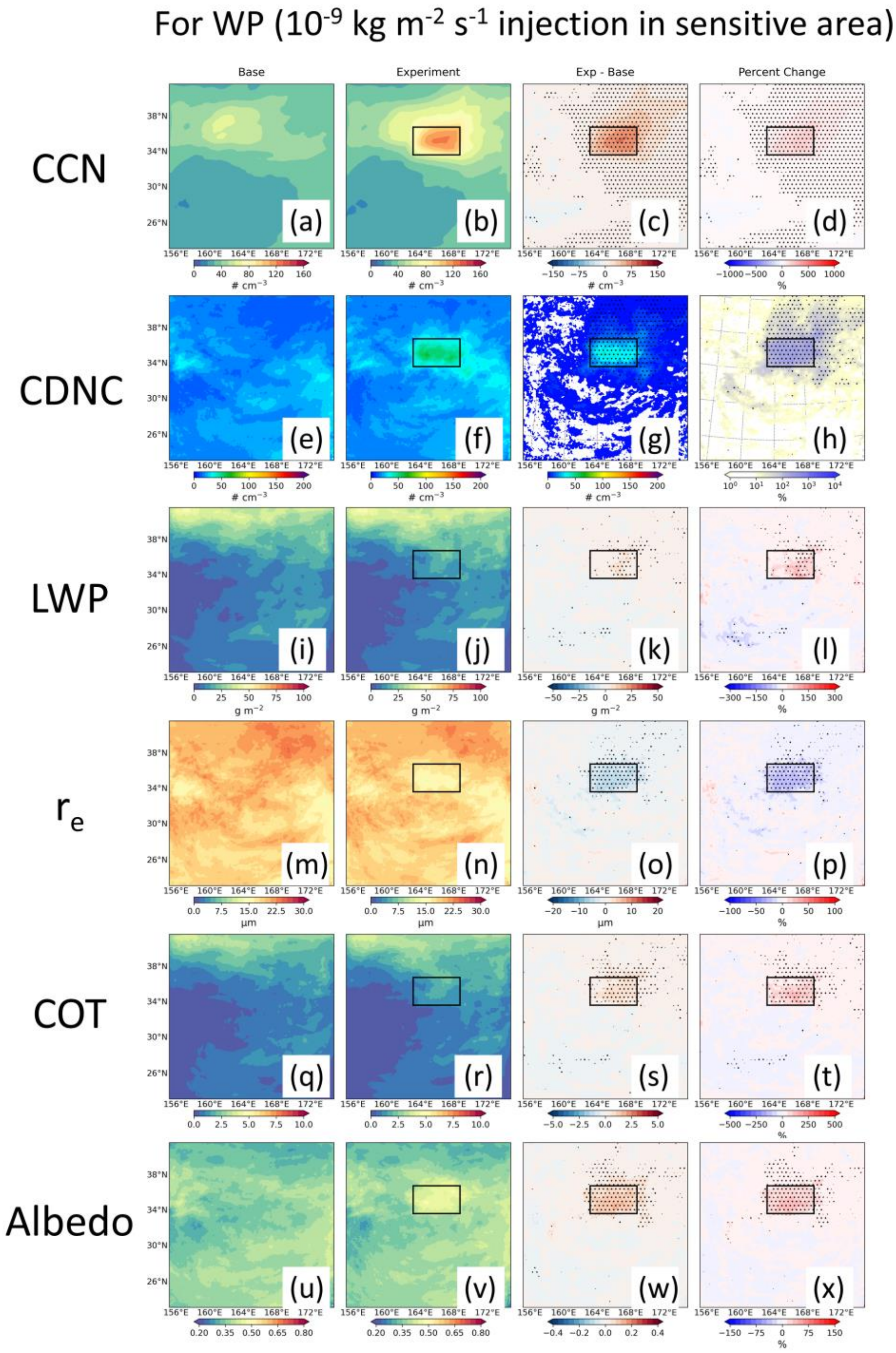

Figure S19. Same caption as Fig. S18, but for the WP region.

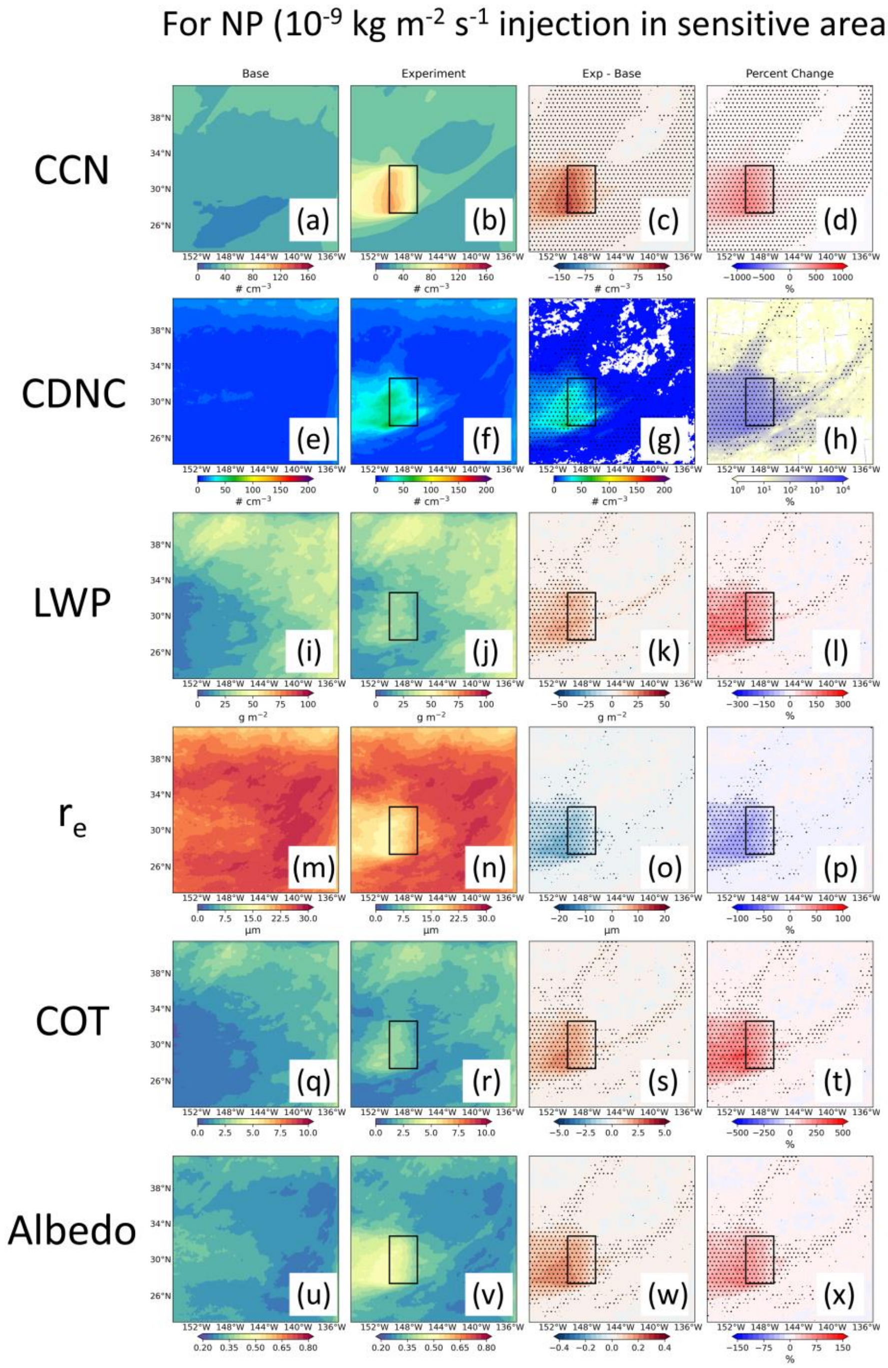

Figure S20. Same caption as Fig. S18, but for the NP region.

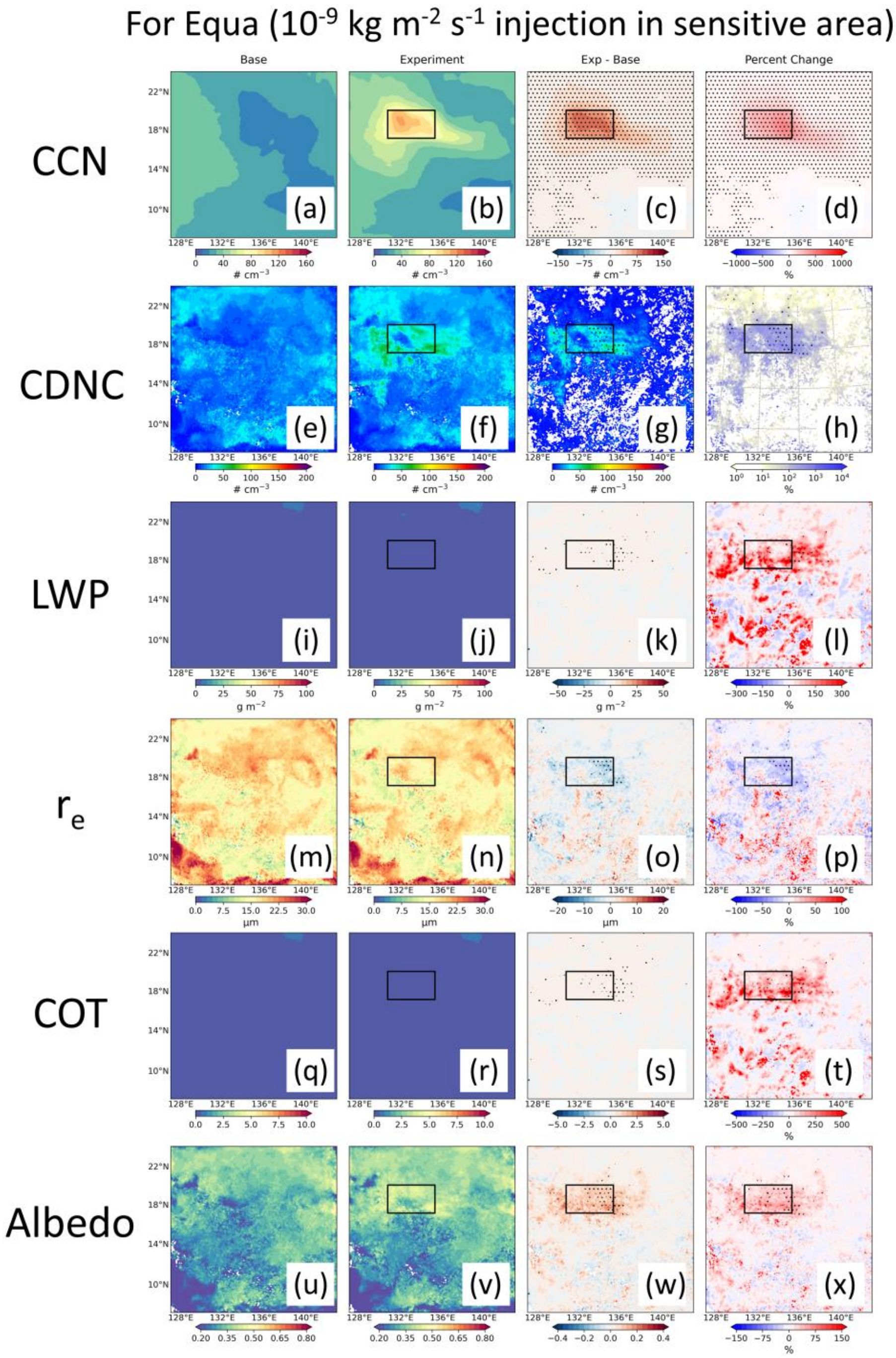

Figure S21. Same caption as Fig. S18, but for the Equa region.

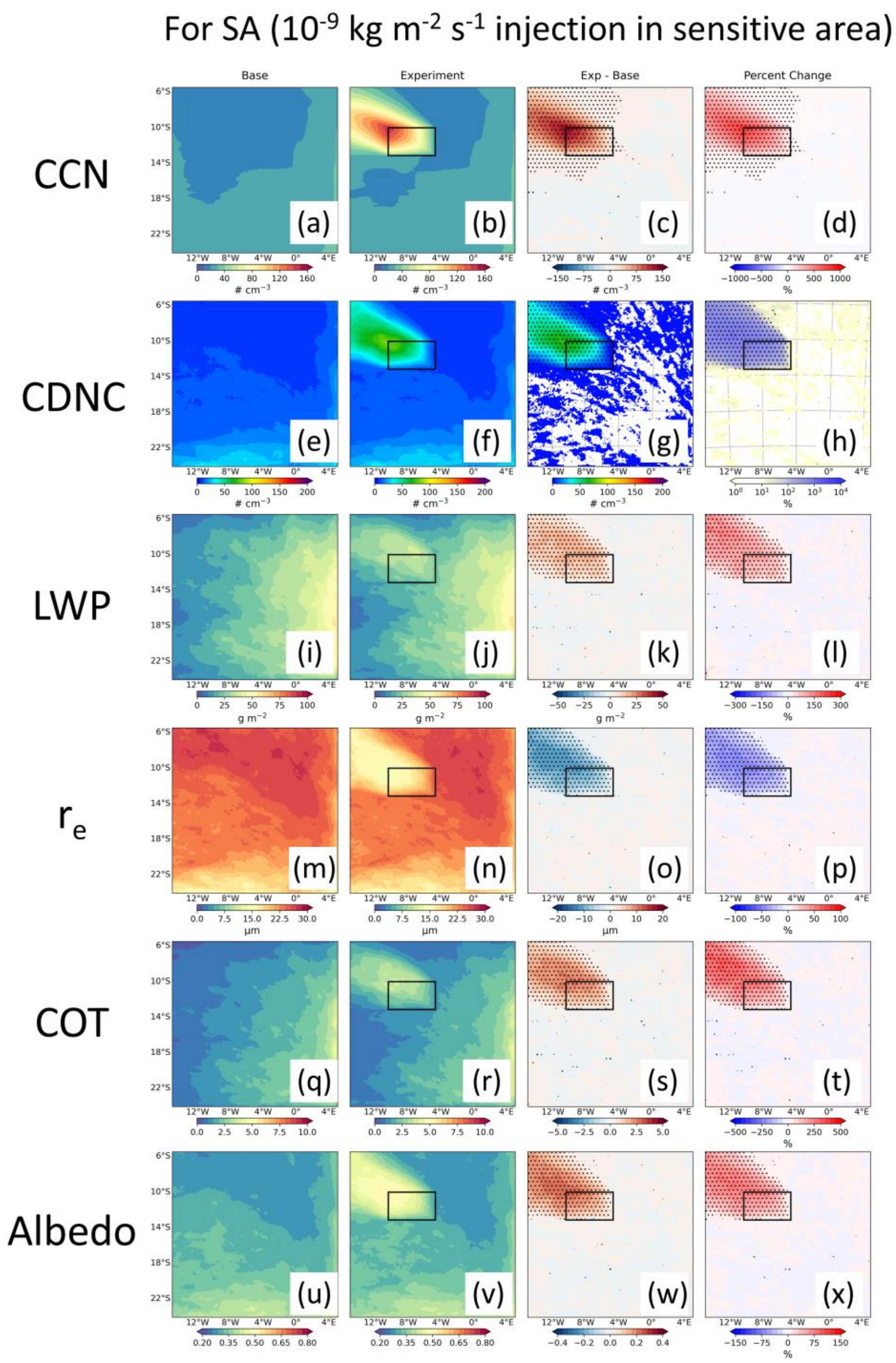

Figure S22. Same caption as Fig. S19, but for the SA region.

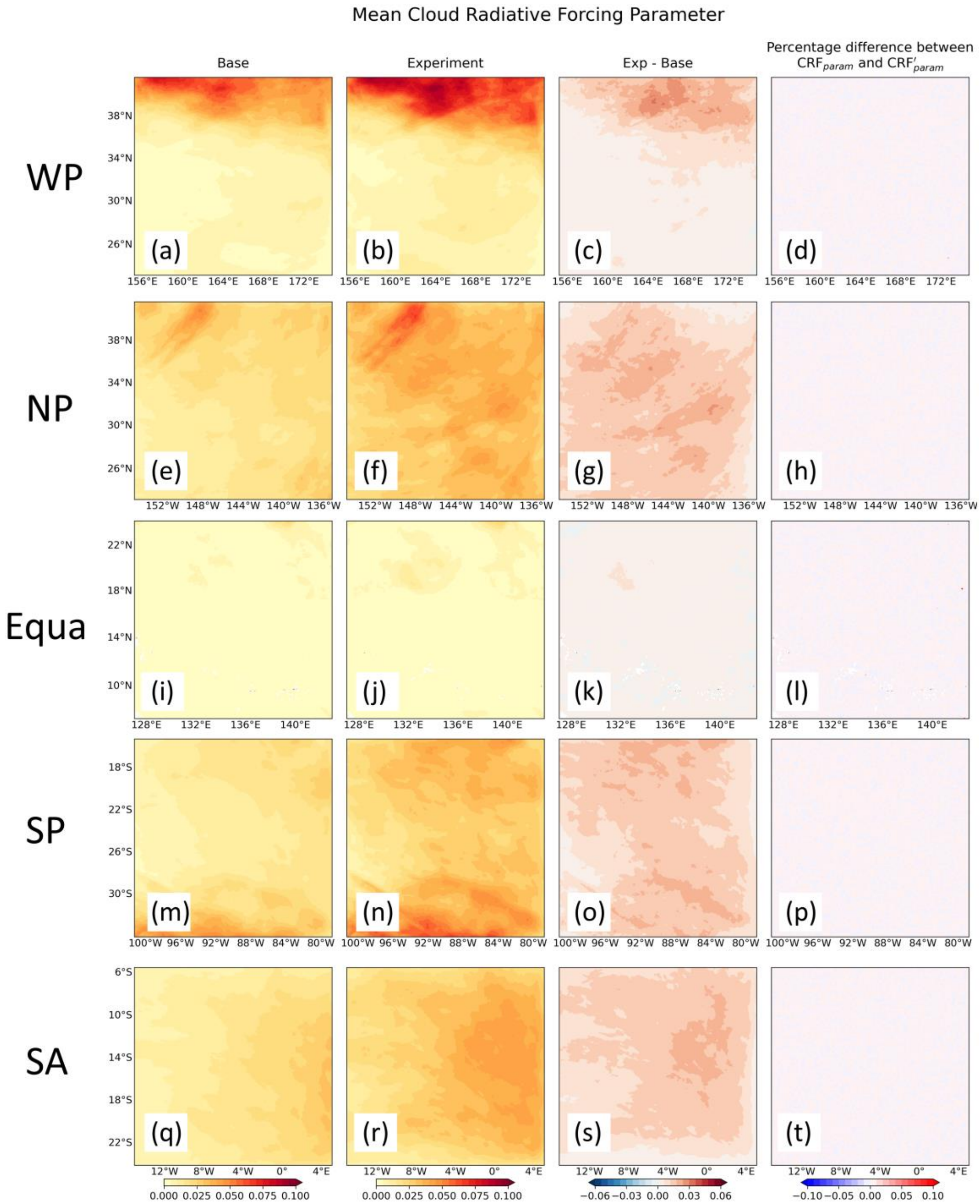

Figure S23. The cloud radiative forcing (CRF) parameters after injection of sea-salt aerosols in the five regions. The first to fourth columns are Base, the sensitivity experiment with a uniform injection of 10^{-9} kg m^{-2} s^{-1} sea-salt aerosols over the entire region, Exp - Base, and the CRF'$_{param}$ approximated by the perturbation method, respectively.

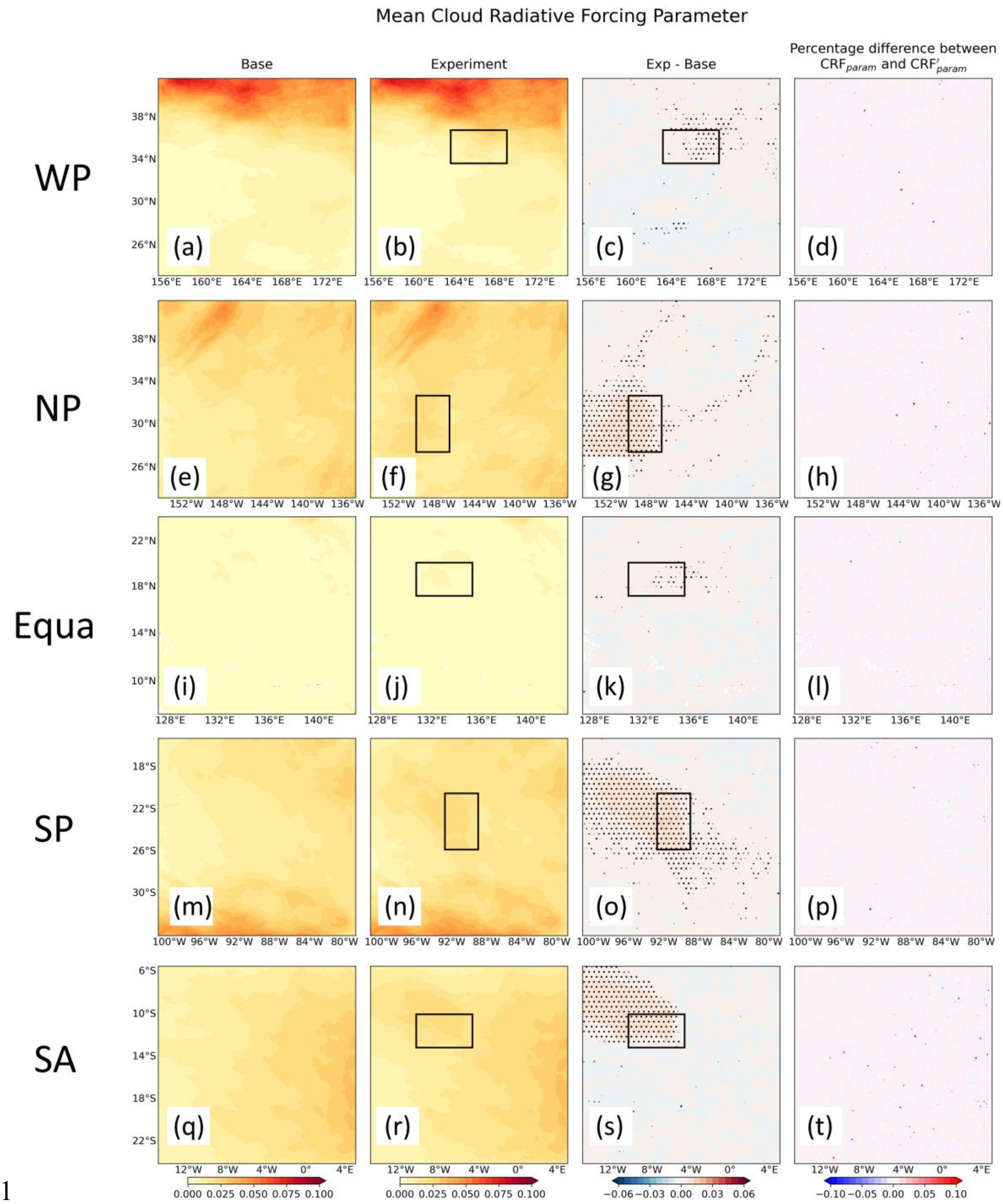

Figure S24. Same caption as Fig. S23, but for the sensitivity experiment with a uniform injection of 10^{-9} kg m^{-2} s^{-1} sea-salt aerosols only in the sensitive area. Areas labeled with dots indicate mean differences that are significant at the 95% confidence level. The black rectangles are sensitive areas.

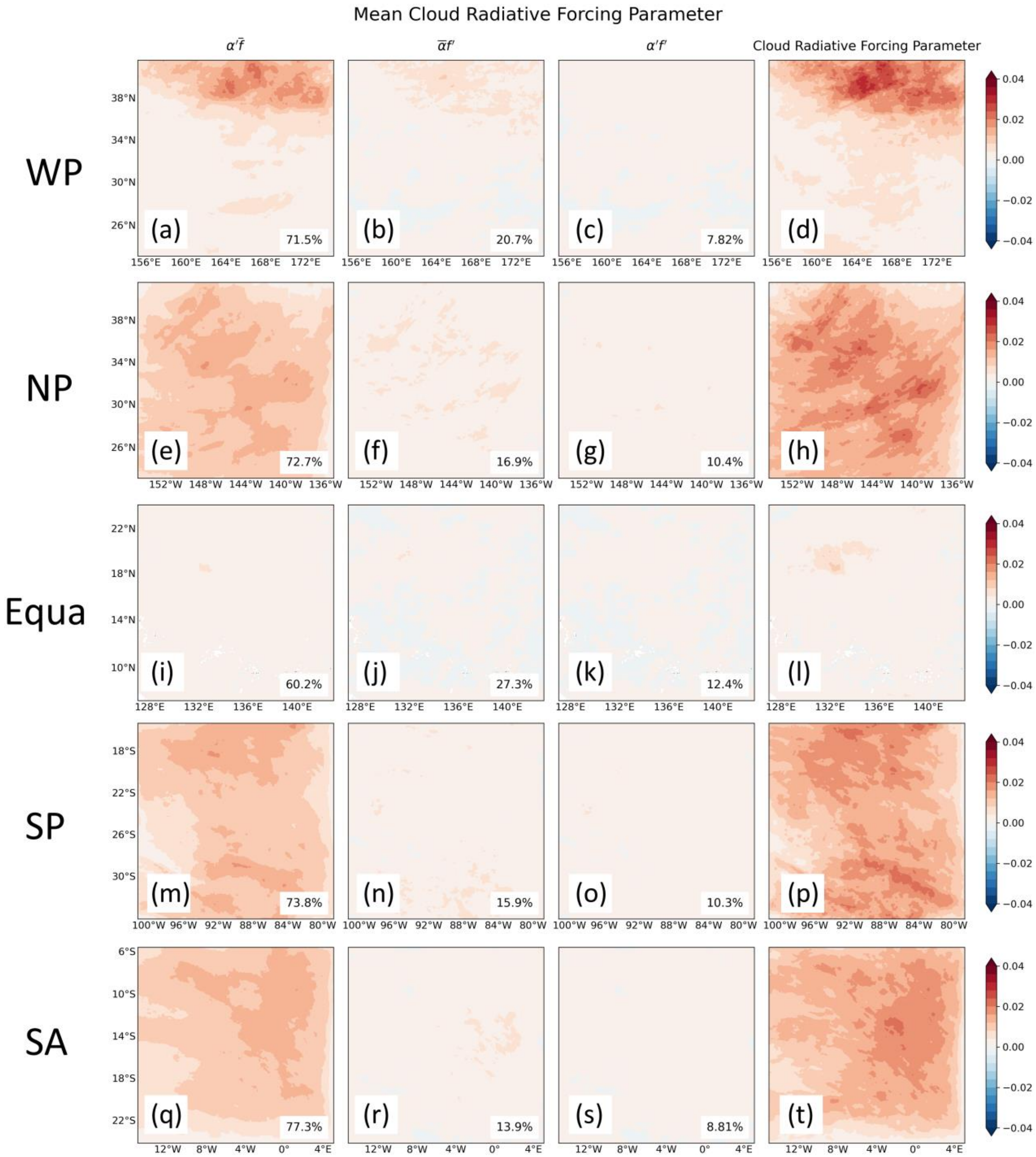

Figure S25. The three additive perturbation terms of the CRF'_{param} after uniform injection of sea-salt aerosols within the five regions (First column: driven by the perturbation of cloud albedo. Second column: driven by the change in cloud fraction. Third column: jointly driven by the interaction of the two.), as well as the CRF'_{param} approximated using the perturbation method (fourth column, see Equation 6 and 7). The percentage contribution of each item to the total CRF'_{param} is labeled in the lower right corner for the entire region.

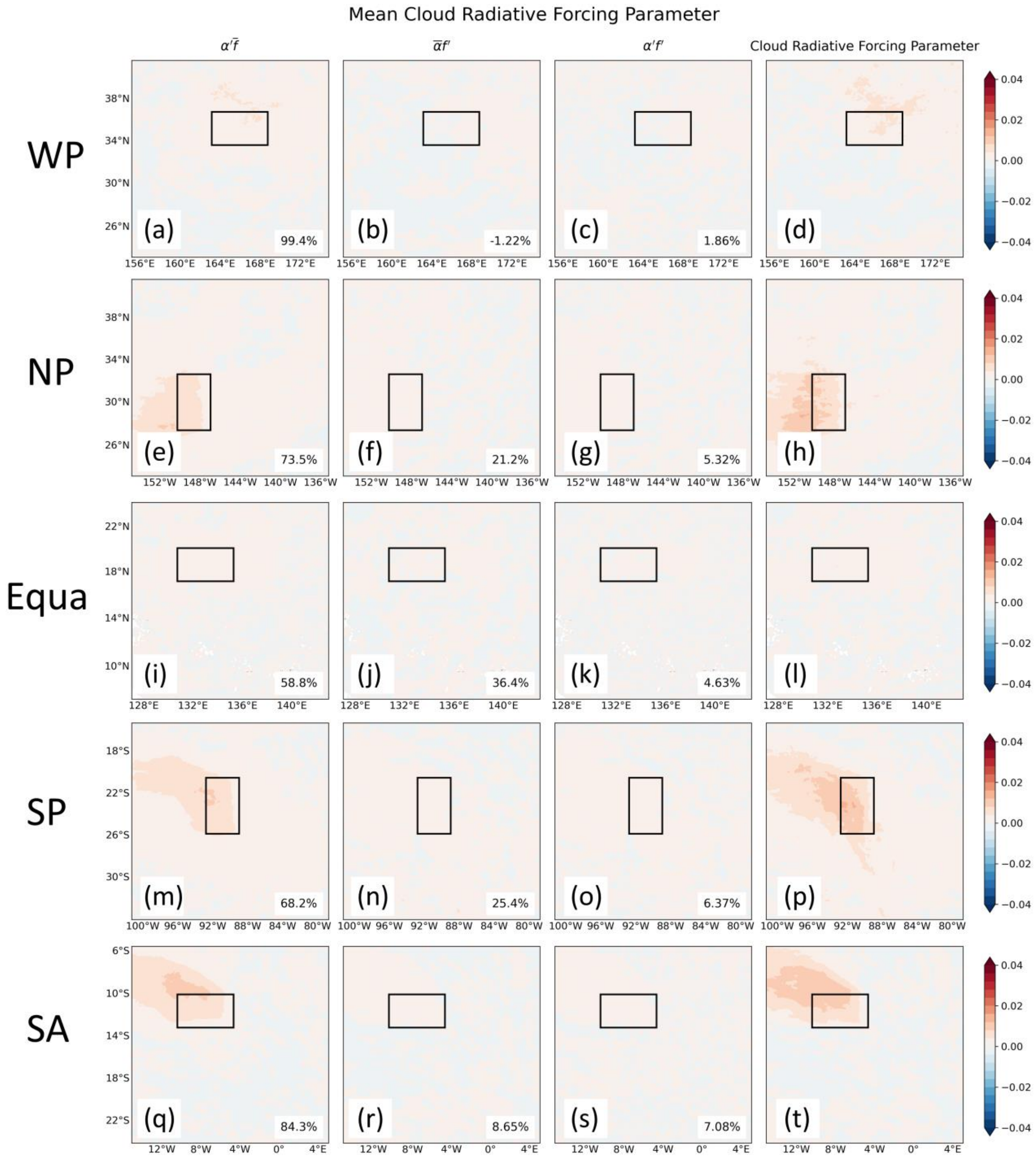

Figure S26. Same caption as Fig. S25, but for the sensitivity experiment with a uniform injection of 10^{-9} kg m^{-2} s^{-1} sea-salt aerosols only in the sensitive area. The black rectangles are sensitive areas.

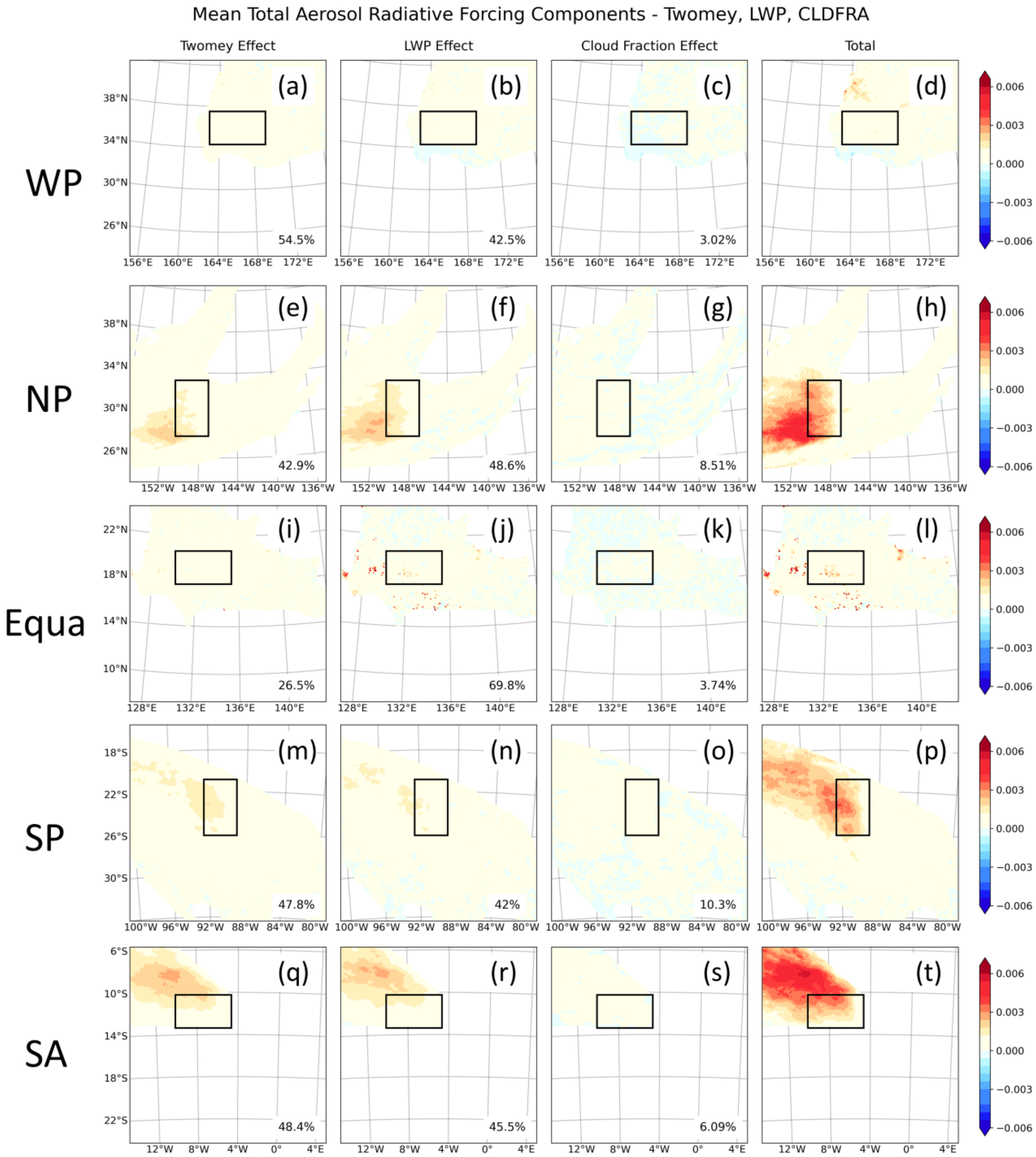

Figure S27. Same caption as Fig. 11, but for the sensitivity experiment with a uniform injection of 10^{-9} kg m^{-2} s^{-1} sea-salt aerosols only in the sensitive area. The black rectangles are sensitive areas.

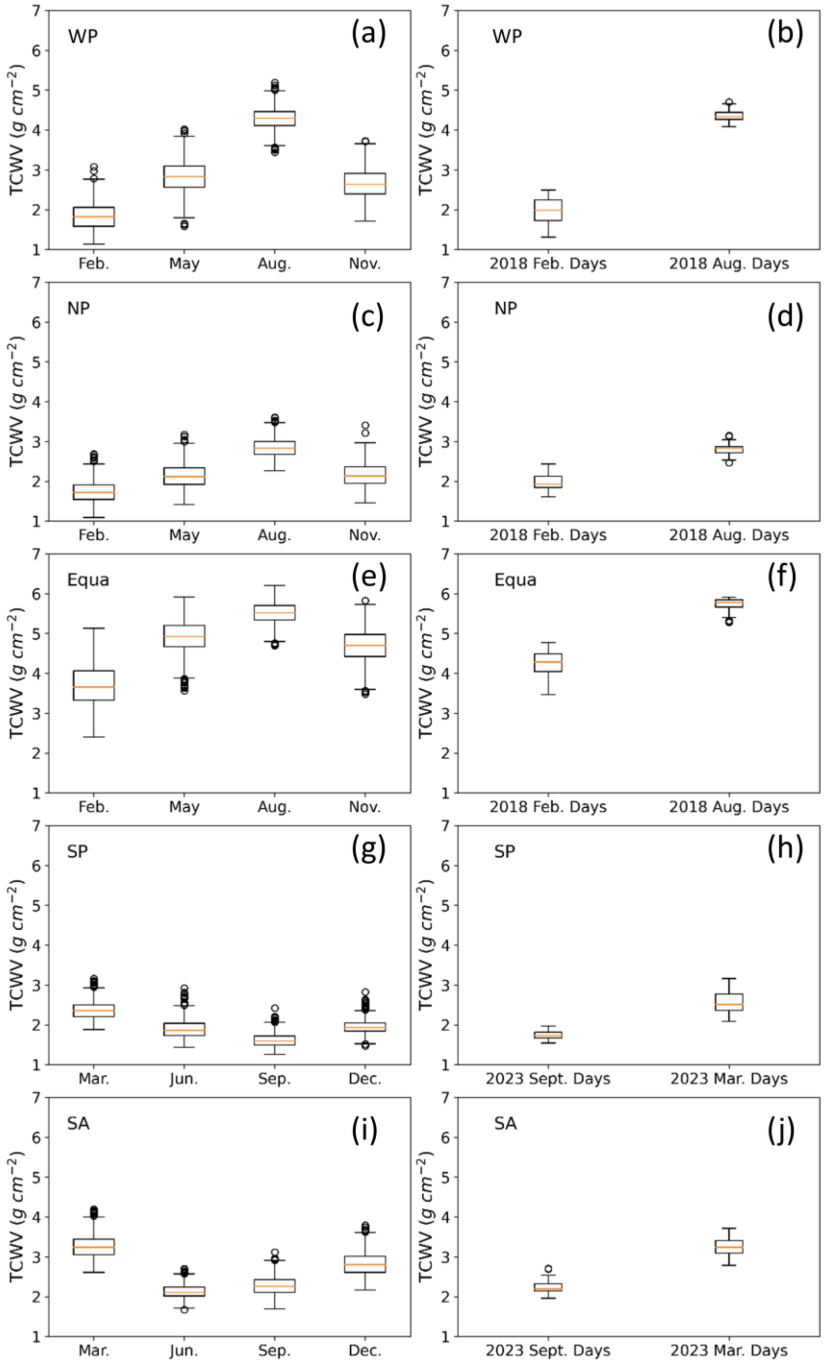

Figure S28. Box plots of total column water vapor (TCWV) for the five ocean regions from ERA5. The left column shows daily mean data from ERA5 for the years 1990–2020 (1990–2023 for SP and SA), listed by month. For WP, NP and Equa, each year is wetter in August and drier in February. For SP and SA, March is wetter and September is drier. The right column shows the daily average of the ERA5 data for the simulated (wetter) and dry months of the year. For WP, NP, and Equa, the initial simulation time period was August 2018, which was wetter, so we chose the dry time period of February of the same year to simulate again. SP and SA were initially simulated in March 2023, which was wetter, so we chose the dry time period of September of the same year to simulate again.

Table S1. Summary of modeling studies on marine cloud brightening (MCB), marine sky brightening (MSB) and injection of sea salt aerosols.

Models	Strategies	Increased emissions	Locations	References
	set N = 400 cm^{-3}	10^9 in mass (NaCl) 10^{26} in number of droplets	global	(Latham, 2002)
A simplified version of the model of marine stratocumulus clouds	ΔN = 10, 30, 100, 300 and 1000 cm^{-3}			(Bower et al., 2006)
HadGAM CAM	set Nd = 375 cm^{-3} set Nd = 375 and 1000 cm^{-3}		global	(Latham et al., 2008)
HadGEM2	set CDNC = 375 cm^{-3}		North Pacific (NP), South Pacific (SP) and South Atlantic (SA)	(Jones et al., 2009)
CCSM	set CDNC = 1000 cm^{-3}		20%, 30%, 40% and 70% of ocean area	(Rasch et al., 2009)
GLOMAP	set geoengineering particle number flux (GEO and 5GEO) according to U10		off the coast of California (North Pacific), Chile (South Pacific), Namibia (South Atlantic) and Western Australia (Indian Ocean)	(Korhonen et al., 2010)
HadGEM2-AO	set CDNC = 375 cm^{-3}		North Pacific (NP), South Pacific (SP) and South Atlantic (SA)	(Jones et al., 2011)
WRF	inject CCN	1.45×10^6 m^{-2} s^{-1} (375 cm^{-3} $hour^{-1}$)		(Wang et al., 2011)
CAM3.5-CLM3.5	r_d over the ocean is reduced from 14 to 11.5 μm		global	(Bala et al., 2011)
NorESM	increase sea-salt emissions	10^{-9} kg m^{-2} s^{-1} (350 tons s^{-1})	global	(Alterskjær et al., 2012)
GFDL-CM2G	set CCN = 500 and 1000 cm^{-3}		North Pacific and the Southern Ocean	(Baughman et al., 2012)
HadGEM1	set CDNC = 375 cm^{-3}		global	(Gadian, 2012)
AGCM	increase sea salt aerosols	fivefold	tropical North Pacific (NP), South Pacific (SP), and South Atlantic (SA)	(Hill and Ming, 2012)
HadGEM2-ES	follow Korhonen et al., (2010)	GEO and 5GEO	global and 10% of optimal sea-spray emission areas	(Jones and Haywood,

				2012)
HadGEM1	set CDNC = 375 cm^{-3}		off the western coasts of California, Peru and Namibia	(Latham et al., 2012a)
HadGEM1	set CDNC = 375 cm^{-3}		global and off the western coasts of California, Peru, Namibia	(Latham et al., 2012b)
ECHAM5.5-HAM2	set geoengineering particle number flux (GEO) according to U10	20.6–443.9 Tg yr^{-1}	global and North Pacific, South Pacific and South Atlantic (3.3% of the Earth's surface)	(Partanen et al., 2012)
0-D model GLOMAP-MODE EMAC ECHAM-HAM	follow Korhonen et al., (2010)		global	(Pringle et al., 2012)
HadGEM1	set CDNC = 375 cm^{-3}		follow Jones et al. (2009)	(Parkes et al., 2012)
NorESM IPSL-CM5A MPI-ESM	increase sea salt aerosols use the output of the NorESM	266–560 Tg yr^{-1}	between 30°S and 30°N	(Alterskjær et al., 2013)
NorESM	increase sea salt emissions	10^{-11}–10^{-8} kg m^{-2} s^{-1}	between 30°S and 30°N	(Alterskjær and Kristjánsson, 2013)
WRF-Chem	inject aerosols	3–15 kg s^{-1}	point source injection	(Jenkins et al., 2013)
MPI-ESM and NorESM	increase sea salt aerosols	10^{-9} kg m^{-2} s^{-1}	between 30°S and 30°N	(Niemeier et al., 2013)
Gaussian plume model LES ECHAM5.5-HAM2	inject aerosols	20.6 Tg yr^{-1}	North Pacific, South Pacific and South Atlantic	(Stuart et al., 2013)
HadGEM2-ES	50% increase in CDNC increase sea salt aerosols	100–400 Tg yr^{-1}	global between 30°S and 30°N	(Kravitz et al., 2013)
Lagrangian Cloud Model	inject aerosols	100, 200, 400, 800 cm^{-3}		(Andrejczuk et al., 2014)
ACPIM	inject aerosols	NaCl mixing ratios= 10^{-14}–		(Connolly et

		10^{-4} kg kg^{-1}		al., 2014)
cloud-resolving model (WRF)	inject CCN	1.45×10^{6} m^{-2} s^{-1}	single moving point source injection (Arctic, 71.32°N, 156.61°W)	(Kravitz et al., 2014)
UCLALES	Inject particles	15 kg s^{-1}		(Maalick et al., 2014)
HadGEM1	set CDNC = 375 cm^{-3}		Antarctic, off the West coasts of North and South America, and Africa	(Latham et al., 2014)
HadGEM2	increase sea salt aerosols	1.8×10^{8} m^{-3}	between 30°S and 30°N	(Crook et al., 2015)
HadGEM1 GLAM	set CDNC = 375 cm^{-3}		off the western coasts of California, Peru and Namibia	(Parkes et al., 2015)
NorESM1-M IPSL-CM5A-LR MPI-ESM-LR	increase sea salt aerosols use the output of the NorESM		between 30°S and 30°N	(Muri et al., 2015)
MPI-ESM NorESM IPSL-CM5	follow Alterskjær et al. (2013) and Muri et al. (2015)		between 30°S and 30°N	(Aswathy et al., 2015)
UVic ESCM ECHAM5.5-HAM2	use the radiative forcing from Partanen et al. (2012)		off the west coasts of North America, South America, and Southern Africa	(Partanen et al., 2016)
LMDZ5B	prescribe an additional concentration sea salt		between 30°S and 30°N	(Boucher et al., 2017)
NorESM1-M GISS-E2-R HadGEM2-ES	inject sea salt particles	250 Tg yr^{-1} 590 Tg yr^{-1} 200 Tg yr^{-1}	between 30°S and 30°N	(Ahlm et al., 2017)
CESM	r_d over the ocean is reduced from 14 to 11 μm		global	(Duan et al., 2018)
NorESM1-ME	increase sea salt emissions	460 Tg yr^{-1}	between 45°S and 45°N	(Muri et al., 2018)
BNU-ESM CanESM2 CSIRO-Mk3L-1-2 GISS-E2-R	set CDNC = 375 cm^{-3}		global	(Stjern et al., 2018)

HadGEM2-ES IPSL-CM5A-LR MIROC-ESM MPI-ESM1-LR NorESM1-M				
BNU-ESM CanESM2 CSIRO-Mk3l-1-2 HadGem2-ES MIROC-ESM	set CDNC = 375 cm^{-3}		global	(Kim et al., 2020)
GEOS-Chem	inject sea salt particles	212–569 Tg yr^{-1} (3.0–8.0×10^{-12} kg m^{-2} s^{-1})	between 30°S and 30°N	(Horowitz et al., 2020)
LCM LES parcel model	inject spray droplets	1.2–18374.9 mg^{-1}		(Hoffmann and Feingold, 2021)
simple heuristic model	inject sea salt particles	50–70 Tg yr^{-1}	54 % of the Earth's surface	(Wood, 2021)
HadGEM2-ES	50% increase in CDNC		the Sahara-Sahel-Arabian Peninsula zone	(Zhu et al., 2021)
CESM	r_d over the ocean is reduced from 14 to 11 µm		global	(Zhao et al., 2021)
BNU-ESM CanESM2 HadGEM2-ES ISPL-CM5A-LR MIROC-ESM NorESM1-M	50% increase in CDNC		global	(Xie et al., 2022)
WRF-Chem	inject sea salt particles	10.8 Tg yr^{-1}	Gulf of Mexico	(Goddard et al., 2022)
GFDL-AM4	increase sea salt emissions	7.66×10^{-11} kg m^{-2} s^{-1} (456 Tg yr^{-1})	between 30°S and 30°N	(Mahfouz et al., 2023)
LCM	inject aerosols	1 µg kg^{-1} of air	25°N, 120°W	(Prabhakaran

LES				et al., 2023)
UKESM1	modify sea salt emissions	413 Tg yr^{-1}	NP (north Pacific: 30°–50°N,170°–240°E), NEP (north-east Pacific: 0°–30°N, 210°–250°E), SEP (south-east Pacific: 0°–30°S, 250°–290°E) and SP (south Pacific: 30°–50°S, 190°–270°E)	(Haywood et al., 2023)

Note: Some studies included multiple sensitivity experiments with aerosol injection, and only representative experiments may be listed in the table.

Table S2. The total upward shortwave radiation flux (SW_TOT) at the TOA and the corresponding sea-salt aerosol injections resulting from different strategies of injecting sea-salt aerosols in five areas, and the MCB efficiency (E_{MCB}).

Strategies	Areas	SW_TOT ($W\ m^{-2}$)	Add Sea-salt aerosols ($\times 10^{-9}\ kg\ m^{-2}\ s^{-1}$)	E_{MCB} ($GW\ kg^{-1}\ s$)
Natural ×5	WP	0.46	0.085	5.33
	NP	2.1	0.057	37.0
	Equa	0.07	0.052	1.40
	SP	1.7	0.034	48.5
	SA	1.4	0.031	43.8
Wind-adjusted	WP	3.8	0.19	20.5
	NP	8.4	0.20	41.1
	Equa	1.4	0.19	7.66
	SP	7.6	0.18	42.2
	SA	8.0	0.21	37.5
Fixed at 10^{-9} kg $m^{-2}\ s^{-1}$	WP	18	0.99	17.7
	NP	23	1.0	23.0
	Equa	11	1.0	10.9
	SP	25	1.0	25.0
	SA	22	1.0	22.5
10^{-9} kg $m^{-2}\ s^{-1}$ in the sensitive area	WP	0.49	0.05	10.2
	NP	2.7	0.05	53.4
	Equa	0.83	0.05	16.5
	SP	3.4	0.05	67.0
	SA	1.7	0.05	34.9
Fixed-wind-adjusted	WP	6.9	1.0	6.88
	NP	16	1.0	16.1
	Equa	5.0	1.0	5.04
	SP	17	1.0	16.6
	SA	20	1.0	19.7

Table S3. Grid coordinates and latitude and longitude ranges of sensitive areas.

Region	Start_x, End_x (in grid)	Start_y, End_y (in grid)	Start_Lat, End_Lat	Start_Lon, End_Lon
WP	(70, 119)	(98, 127)	(28.18, 31.66)	(156.7, 162.6)
NP	(40, 69)	(40, 89)	(24.86, 30.34)	(-153.4, -150.5)
Equa	(40, 89)	(103, 132)	(18.15, 21.25)	(130.0, 135.2)
SP	(65, 94)	(75, 124)	(-26.18, -20.84)	(-92.56, -89.06)
SA	(40, 89)	(101, 130)	(-13.77, -10.76)	(-13.03, -7.530)

References

Ahlm, L., Jones, A., Stjern, C. W., Muri, H., Kravitz, B., and Kristjánsson, J. E.: Marine cloud brightening – as effective without clouds, Atmospheric Chemistry and Physics, 17, 13071–13087, https://doi.org/10.5194/acp-17-13071-2017, 2017.

Alterskjær, K. and Kristjánsson, J. E.: The sign of the radiative forcing from marine cloud brightening depends on both particle size and injection amount, Geophysical Research Letters, 40, 210–215, https://doi.org/10.1029/2012GL054286, 2013.

Alterskjær, K., Kristjánsson, J. E., and Seland, Ø.: Sensitivity to deliberate sea salt seeding of marine clouds – observations and model simulations, Atmospheric Chemistry and Physics, 12, 2795–2807, https://doi.org/10.5194/acp-12-2795-2012, 2012.

Alterskjær, K., Kristjánsson, J. E., Boucher, O., Muri, H., Niemeier, U., Schmidt, H., Schulz, M., and Timmreck, C.: Sea-salt injections into the low-latitude marine boundary layer: The transient response in three Earth system models, Journal of Geophysical Research: Atmospheres, 118, 12,195-12,206, https://doi.org/10.1002/2013JD020432, 2013.

Andrejczuk, M., Gadian, A., and Blyth, A.: Numerical simulations of stratocumulus cloud response to aerosol perturbation, Atmospheric Research, 140–141, 76–84, https://doi.org/10.1016/j.atmosres.2014.01.006, 2014.

Aswathy, V. N., Boucher, O., Quaas, M., Niemeier, U., Muri, H., Mülmenstädt, J., and Quaas, J.: Climate extremes in multi-model simulations of stratospheric aerosol and marine cloud brightening climate engineering, Atmospheric Chemistry and Physics, 15, 9593–9610, https://doi.org/10.5194/acp-15-9593-2015, 2015.

Bala, G., Caldeira, K., Nemani, R., Cao, L., Ban-Weiss, G., and Shin, H.-J.: Albedo enhancement of marine clouds to counteract global warming: impacts on the hydrological cycle, Clim Dyn, 37, 915–931, https://doi.org/10.1007/s00382-010-0868-1, 2011.

Baughman, E., Gnanadesikan, A., Degaetano, A., and Adcroft, A.: Investigation of the Surface and Circulation Impacts of Cloud-Brightening Geoengineering, Journal of Climate, 25, 7527–7543, https://doi.org/10.1175/JCLI-D-11-00282.1, 2012.

Boucher, O., Kleinschmitt, C., and Myhre, G.: Quasi-Additivity of the Radiative Effects of Marine Cloud Brightening and Stratospheric Sulfate Aerosol Injection, Geophysical Research Letters, 44, 11,158-11,165, https://doi.org/10.1002/2017GL074647, 2017.

Bower, K., Choularton, T., Latham, J., Sahraei, J., and Salter, S.: Computational assessment of a proposed technique for global warming mitigation via albedo-enhancement of marine stratocumulus clouds, Atmospheric Research, 82, 328–336, https://doi.org/10.1016/j.atmosres.2005.11.013, 2006.

Connolly, P. J., McFiggans, G. B., Wood, R., and Tsiamis, A.: Factors determining the most efficient spray distribution for marine cloud brightening, Philosophical Transactions of the Royal Society A: Mathematical, Physical and Engineering Sciences, 372, 20140056, https://doi.org/10.1098/rsta.2014.0056, 2014.

Crook, J. A., Jackson, L. S., Osprey, S. M., and Forster, P. M.: A comparison of temperature and precipitation responses to different Earth radiation management geoengineering schemes, Journal of Geophysical Research: Atmospheres, 120, 9352–9373, https://doi.org/10.1002/2015JD023269, 2015.

Duan, L., Cao, L., Bala, G., and Caldeira, K.: Comparison of the Fast and Slow Climate Response to Three Radiation Management Geoengineering Schemes, Journal of Geophysical Research: Atmospheres, 123, 11,980-12,001, https://doi.org/10.1029/2018JD029034, 2018.

Gadian, A.: Marine cloud brightening: the effect on global surface temperatures, Journal of Earth Science & Climatic Change, 01, https://doi.org/10.4172/2157-7617.S1.002, 2012.

Goddard, P. B., Kravitz, B., MacMartin, D. G., and Wang, H.: The Shortwave Radiative Flux Response to an Injection of Sea Salt Aerosols in the Gulf of Mexico, Journal of Geophysical Research: Atmospheres, 127, e2022JD037067, https://doi.org/10.1029/2022JD037067, 2022.

Haywood, J. M., Jones, A., Jones, A. C., and Rasch, P. J.: Climate Intervention using marine cloud brightening (MCB) compared with stratospheric aerosol injection (SAI) in the UKESM1 climate model, EGUsphere, 1–38, https://doi.org/10.5194/egusphere-2023-1611, 2023.

Hill, S. and Ming, Y.: Nonlinear climate response to regional brightening of tropical marine stratocumulus, Geophysical Research Letters, 39, https://doi.org/10.1029/2012GL052064, 2012.

Hoffmann, F. and Feingold, G.: Cloud Microphysical Implications for Marine Cloud Brightening: The Importance of the Seeded Particle Size Distribution, Journal of the Atmospheric Sciences, 78, 3247–3262, https://doi.org/10.1175/JAS-D-21-0077.1, 2021.

Horowitz, H. M., Holmes, C., Wright, A., Sherwen, T., Wang, X., Evans, M., Huang, J., Jaeglé, L., Chen, Q., Zhai, S., and Alexander, B.: Effects of Sea Salt Aerosol Emissions for Marine Cloud Brightening on Atmospheric Chemistry: Implications for Radiative Forcing, Geophysical Research Letters, 47, e2019GL085838, https://doi.org/10.1029/2019GL085838, 2020.

Jenkins, A. K. L., Forster, P. M., and Jackson, L. S.: The effects of timing and rate of marine cloud brightening aerosol injection on albedo changes during the diurnal cycle of marine stratocumulus clouds, Atmospheric Chemistry and Physics, 13, 1659–1673, https://doi.org/10.5194/acp-13-1659-2013, 2013.

Jones, A. and Haywood, J. M.: Sea-spray geoengineering in the HadGEM2-ES earth-system model: radiative impact and climate response, Atmospheric Chemistry and Physics, 12, 10887–10898, https://doi.org/10.5194/acp-12-10887-2012, 2012.

Jones, A., Haywood, J., and Boucher, O.: Climate impacts of geoengineering marine stratocumulus clouds, Journal of Geophysical Research: Atmospheres, 114, https://doi.org/10.1029/2008JD011450, 2009.

Jones, A., Haywood, J., and Boucher, O.: A comparison of the climate impacts of geoengineering by stratospheric SO2 injection and by brightening of marine stratocumulus cloud, Atmospheric Science Letters, 12, 176–183, https://doi.org/10.1002/asl.291, 2011.

Kim, D.-H., Shin, H.-J., and Chung, I.-U.: Geoengineering: Impact of Marine Cloud Brightening Control on the Extreme Temperature Change over East Asia, Atmosphere, 11, 1345, https://doi.org/10.3390/atmos11121345, 2020.

Korhonen, H., Carslaw, K. S., and Romakkaniemi, S.: Enhancement of marine cloud albedo via controlled sea spray injections: a global model study of the influence of emission rates, microphysics and transport, Atmospheric Chemistry and Physics, 10, 4133–4143, https://doi.org/10.5194/acp-10-4133-2010, 2010.

Kravitz, B., Forster, P. M., Jones, A., Robock, A., Alterskjær, K., Boucher, O., Jenkins, A. K. L., Korhonen, H., Kristjánsson, J. E., Muri, H., Niemeier, U., Partanen, A.-I., Rasch, P. J., Wang, H., and Watanabe, S.: Sea spray geoengineering experiments in the geoengineering model intercomparison project (GeoMIP): Experimental design and preliminary results, Journal of Geophysical Research: Atmospheres, 118, 11,175-11,186, https://doi.org/10.1002/jgrd.50856, 2013.

Kravitz, B., Wang, H., Rasch, P. J., Morrison, H., and Solomon, A. B.: Process-model simulations of cloud albedo enhancement by aerosols in the Arctic, Phil. Trans. R. Soc. A., 372, 20140052, https://doi.org/10.1098/rsta.2014.0052, 2014.

Latham, J.: Amelioration of global warming by controlled enhancement of the albedo and longevity of low-level maritime clouds, Atmospheric Science Letters, 3, 52–58, https://doi.org/10.1006/asle.2002.0048, 2002.

Latham, J., Rasch, P., Chen, C.-C., Kettles, L., Gadian, A., Gettelman, A., Morrison, H., Bower, K., and Choularton, T.: Global temperature stabilization via controlled albedo enhancement of low-level maritime clouds, Philosophical Transactions of the Royal Society A: Mathematical, Physical and Engineering Sciences, 366, 3969–3987, https://doi.org/10.1098/rsta.2008.0137, 2008.

Latham, J., Bower, K., Choularton, T., Coe, H., Connolly, P., Cooper, G., Craft, T., Foster, J., Gadian, A., Galbraith, L., Iacovides, H., Johnston, D., Launder, B., Leslie, B., Meyer, J., Neukermans, A., Ormond, B., Parkes, B., Rasch, P., Rush, J., Salter, S., Stevenson, T., Wang, H., Wang, Q., and Wood, R.: Marine cloud brightening, Philosophical Transactions of the Royal Society A: Mathematical, Physical and Engineering Sciences, 370, 4217–4262, https://doi.org/10.1098/rsta.2012.0086, 2012a.

Latham, J., Parkes, B., Gadian, A., and Salter, S.: Weakening of hurricanes via marine cloud brightening (MCB), Atmospheric Science Letters, 13, 231–237, https://doi.org/10.1002/asl.402, 2012b.

Latham, J., Gadian, A., Fournier, J., Parkes, B., Wadhams, P., and Chen, J.: Marine cloud brightening: regional applications, Philosophical Transactions of the Royal Society A: Mathematical, Physical and Engineering Sciences, 372, 20140053, https://doi.org/10.1098/rsta.2014.0053, 2014.

Maalick, Z., Korhonen, H., Kokkola, H., Kühn, T., and Romakkaniemi, S.: Modelling artificial sea salt emission in large eddy simulations, Philosophical Transactions of the Royal Society A: Mathematical, Physical and Engineering Sciences, 372, 20140051, https://doi.org/10.1098/rsta.2014.0051, 2014.

Mahfouz, N. G. A., Hill, S. A., Guo, H., and Ming, Y.: The Radiative and Cloud Responses to Sea Salt Aerosol Engineering in GFDL Models, Geophysical Research Letters, 50, e2022GL102340, https://doi.org/10.1029/2022GL102340, 2023.

Martin, G. M., Johnson, D. W., and Spice, A.: The Measurement and Parameterization of Effective Radius of Droplets in Warm Stratocumulus Clouds, Journal of the Atmospheric Sciences, 51, 1823–1842, https://doi.org/10.1175/1520-0469(1994)051<1823:TMAPOE>2.0.CO;2, 1994.

Muri, H., Niemeier, U., and Kristjánsson, J. E.: Tropical rainforest response to marine sky brightening climate engineering, Geophysical Research Letters, 42, 2951–2960, https://doi.org/10.1002/2015GL063363, 2015.

Muri, H., Tjiputra, J., Otterå, O. H., Adakudlu, M., Lauvset, S. K., Grini, A., Schulz, M., Niemeier, U., and Kristjánsson, J. E.: Climate Response to Aerosol Geoengineering: A Multimethod Comparison, Journal of Climate, 31, 6319–6340, https://doi.org/10.1175/JCLI-D-17-0620.1, 2018.

Niemeier, U., Schmidt, H., Alterskjær, K., and Kristjánsson, J. E.: Solar irradiance reduction via climate engineering: Impact of different techniques on the energy balance and the hydrological cycle, Journal of Geophysical Research: Atmospheres, 118, 11,905-11,917, https://doi.org/10.1002/2013JD020445, 2013.

Parkes, B., Gadian, A., and Latham, J.: The Effects of Marine Cloud Brightening on Seasonal Polar Temperatures and the Meridional Heat Flux, International Scholarly Research Notices, 2012, e142872, https://doi.org/10.5402/2012/142872, 2012.

Parkes, B., Challinor, A., and Nicklin, K.: Crop failure rates in a geoengineered climate: impact of climate change and marine cloud brightening, Environ. Res. Lett., 10, 084003, https://doi.org/10.1088/1748-9326/10/8/084003, 2015.

Partanen, A.-I., Kokkola, H., Romakkaniemi, S., Kerminen, V.-M., Lehtinen, K. E. J., Bergman, T., Arola, A., and Korhonen, H.: Direct and indirect effects of sea spray geoengineering and the role of injected particle size, Journal of Geophysical Research: Atmospheres, 117, https://doi.org/10.1029/2011JD016428, 2012.

Partanen, A.-I., Keller, D. P., Korhonen, H., and Matthews, H. D.: Impacts of sea spray geoengineering on ocean biogeochemistry, Geophysical Research Letters, 43, 7600–7608, https://doi.org/10.1002/2016GL070111, 2016.

Prabhakaran, P., Hoffmann, F., and Feingold, G.: Evaluation of Pulse Aerosol Forcing on Marine Stratocumulus Clouds in the Context of Marine Cloud Brightening, Journal of the Atmospheric Sciences, 80, 1585–1604, https://doi.org/10.1175/JAS-D-22-0207.1, 2023.

Pringle, K. J., Carslaw, K. S., Fan, T., Mann, G. W., Hill, A., Stier, P., Zhang, K., and Tost, H.: A multi-model assessment of the impact of sea spray geoengineering on cloud droplet number, Atmospheric Chemistry and Physics, 12, 11647–11663, https://doi.org/10.5194/acp-12-11647-2012, 2012.

Rasch, P. J., Latham, J., and Chen, C.-C. (Jack): Geoengineering by cloud seeding: influence on sea ice and climate system, Environ. Res. Lett., 4, 045112, https://doi.org/10.1088/1748-9326/4/4/045112, 2009.

Schwartz, S. E., Harshvardhan, and Benkovitz, C. M.: Influence of anthropogenic aerosol on cloud optical depth and albedo shown by satellite measurements and chemical transport modeling, Proceedings of the National Academy of Sciences, 99, 1784–1789, https://doi.org/10.1073/pnas.261712099, 2002.

Stephens, G. L.: Radiation Profiles in Extended Water Clouds. II: Parameterization Schemes, Journal of the Atmospheric Sciences, 35, 2123–2132, https://doi.org/10.1175/1520-0469(1978)035<2123:RPIEWC>2.0.CO;2, 1978.

Stjern, C. W., Muri, H., Ahlm, L., Boucher, O., Cole, J. N. S., Ji, D., Jones, A., Haywood, J., Kravitz, B., Lenton, A., Moore, J. C., Niemeier, U., Phipps, S. J., Schmidt, H., Watanabe, S., and Kristjánsson, J. E.: Response to marine cloud brightening in a multi-model ensemble, Atmospheric Chemistry and Physics, 18, 621–634, https://doi.org/10.5194/acp-18-621-2018, 2018.

Stuart, G. S., Stevens, R. G., Partanen, A.-I., Jenkins, A. K. L., Korhonen, H., Forster, P. M., Spracklen, D. V., and Pierce, J. R.: Reduced efficacy of marine cloud brightening geoengineering due to in-plume aerosol coagulation: parameterization and global implications, Atmospheric Chemistry and Physics, 13, 10385–10396, https://doi.org/10.5194/acp-13-10385-2013, 2013.

Wang, H., Rasch, P. J., and Feingold, G.: Manipulating marine stratocumulus cloud amount and albedo: a process-modelling study of aerosol-cloud-precipitation interactions in response to injection of cloud condensation nuclei, Atmospheric Chemistry and Physics, 11, 4237–4249, https://doi.org/10.5194/acp-11-4237-2011, 2011.

Wood, R.: Cancellation of Aerosol Indirect Effects in Marine Stratocumulus through Cloud Thinning, Journal of the Atmospheric Sciences, 64, 2657–2669, https://doi.org/10.1175/JAS3942.1, 2007.

Wood, R.: Assessing the potential efficacy of marine cloud brightening for cooling Earth using a simple heuristic model, Atmospheric Chemistry and Physics, 21, 14507–14533, https://doi.org/10.5194/acp-21-14507-2021, 2021.

Xie, M., Moore, J. C., Zhao, L., Wolovick, M., and Muri, H.: Impacts of three types of solar geoengineering on the Atlantic Meridional Overturning Circulation, Atmospheric Chemistry and Physics, 22, 4581–4597, https://doi.org/10.5194/acp-22-4581-2022, 2022.

Zhao, M., Cao, L., Duan, L., Bala, G., and Caldeira, K.: Climate More Responsive to Marine Cloud Brightening Than Ocean Albedo Modification: A Model Study, Journal of Geophysical Research: Atmospheres, 126, e2020JD033256, https://doi.org/10.1029/2020JD033256, 2021.

Zhu, Y., Zhang, Z., and Crabbe, M. J. C.: Extreme climate response to marine cloud brightening in the arid Sahara-Sahel-Arabian Peninsula zone, International Journal of Climate Change Strategies and Management, 13, 250–265, https://doi.org/10.1108/IJCCSM-06-2020-0051, 2021.